NASA/TP—2015-216588

Assessment of Technologies for Noncryogenic Hybrid Electric Propulsion

Timothy P. Dever
Glenn Research Center, Cleveland, Ohio

Kirsten P. Duffy
University of Toledo, Cleveland, Ohio

Andrew J. Provenza, Patricia L. Loyselle, Benjamin B. Choi, and Carlos R. Morrison
Glenn Research Center, Cleveland, Ohio

Angela M. Lowe
Aerospace Systems Design Laboratory (ASDL), Georgia Institute of Technology, Atlanta, Georgia

January 2015

NASA STI Program . . . in Profile

Since its founding, NASA has been dedicated to the advancement of aeronautics and space science. The NASA Scientific and Technical Information (STI) program plays a key part in helping NASA maintain this important role.

The NASA STI Program operates under the auspices of the Agency Chief Information Officer. It collects, organizes, provides for archiving, and disseminates NASA's STI. The NASA STI program provides access to the NASA Aeronautics and Space Database and its public interface, the NASA Technical Reports Server, thus providing one of the largest collections of aeronautical and space science STI in the world. Results are published in both non-NASA channels and by NASA in the NASA STI Report Series, which includes the following report types:

- TECHNICAL PUBLICATION. Reports of completed research or a major significant phase of research that present the results of NASA programs and include extensive data or theoretical analysis. Includes compilations of significant scientific and technical data and information deemed to be of continuing reference value. NASA counterpart of peer-reviewed formal professional papers but has less stringent limitations on manuscript length and extent of graphic presentations.

- TECHNICAL MEMORANDUM. Scientific and technical findings that are preliminary or of specialized interest, e.g., quick release reports, working papers, and bibliographies that contain minimal annotation. Does not contain extensive analysis.

- CONTRACTOR REPORT. Scientific and technical findings by NASA-sponsored contractors and grantees.

- CONFERENCE PUBLICATION. Collected papers from scientific and technical conferences, symposia, seminars, or other meetings sponsored or cosponsored by NASA.

- SPECIAL PUBLICATION. Scientific, technical, or historical information from NASA programs, projects, and missions, often concerned with subjects having substantial public interest.

- TECHNICAL TRANSLATION. English-language translations of foreign scientific and technical material pertinent to NASA's mission.

Specialized services also include organizing and publishing research results, distributing specialized research announcements and feeds, providing information desk and personal search support, and enabling data exchange services.

For more information about the NASA STI program, see the following:

- Access the NASA STI program home page at *http://www.sti.nasa.gov*

- E-mail your question to *help@sti.nasa.gov*

- Phone the NASA STI Information Desk at 757-864-9658

- Write to:
  NASA STI Information Desk
  Mail Stop 148
  NASA Langley Research Center
  Hampton, VA 23681-2199

NASA/TP—2015-216588

Assessment of Technologies for Noncryogenic Hybrid Electric Propulsion

Timothy P. Dever
Glenn Research Center, Cleveland, Ohio

Kirsten P. Duffy
University of Toledo, Cleveland, Ohio

Andrew J. Provenza, Patricia L. Loyselle, Benjamin B. Choi, and Carlos R. Morrison
Glenn Research Center, Cleveland, Ohio

Angela M. Lowe
Aerospace Systems Design Laboratory (ASDL), Georgia Institute of Technology, Atlanta, Georgia

National Aeronautics and
Space Administration

Glenn Research Center
Cleveland, Ohio 44135

January 2015

Acknowledgments

Permissions have been obtained from the copyright holders to use
Figures 3 to 5, 9 to 17, 19, 20, 23 to 25, 28, 33, 39, 53, and 54. See figure captions for details.

This work was sponsored by the Fundamental Aeronautics Program at the NASA Glenn Research Center.

Level of Review: This material has been technically reviewed by a committee of peers.

Available from

NASA STI Information Desk
Mail Stop 148
NASA Langley Research Center
Hampton, VA 23681-2199

National Technical Information Service
5301 Shawnee Road
Alexandria, VA 22312

Available electronically at http://www.sti.nasa.gov

Content

Assessment of Technologies for Noncryogenic Hybrid Electric Propulsion

Timothy P. Dever
National Aeronautics and Space Administration
Glenn Research Center
Cleveland, Ohio 44135

Kirsten P. Duffy
University of Toledo
Cleveland, Ohio 44135

Andrew J. Provenza, Patricia L. Loyselle, Benjamin B. Choi, and Carlos R. Morrison
National Aeronautics and Space Administration
Glenn Research Center
Cleveland, Ohio 44135

Angela M. Lowe
Aerospace Systems Design Laboratory (ASDL)
Georgia Institute of Technology
Atlanta, Georgia 30332

Summary

The Subsonic Fixed Wing Project of NASA's Fundamental Aeronautics Program is researching aircraft propulsion technologies that will lower noise, emissions, and fuel burn. One promising technology is noncryogenic electric propulsion, which could be either hybrid electric propulsion or turboelectric propulsion. Reducing dependence on the turbine engine would certainly reduce emissions. However, the weight of the electric-motor-related components that would have to be added would adversely impact the benefits of the smaller turbine engine. Therefore, research needs to be done to improve component efficiencies and reduce component weights. This study projects technology improvements expected in the next 15 and 30 years, including motor-related technologies, power electronics, and energy-storage-related technologies. Motor efficiency and power density could be increased through the use of better conductors, insulators, magnets, bearings, structural materials, and thermal management. Energy storage could be accomplished through batteries, flywheels, or supercapacitors, all of which expect significant energy density growth over the next few decades. A first-order approximation of the cumulative effect of each technology improvement shows that motor power density could be improved from 3 hp/lb, the state of the art, to 8 hp/lb in 15 years and 16 hp/lb in 30 years.

1.0 Introduction

The Subsonic Fixed Wing Project of NASA's Fundamental Aeronautics Program is researching aircraft propulsion technologies that will lower noise, emissions, and fuel burn. One promising technology is electric propulsion, which could be either hybrid electric propulsion or turboelectric propulsion. In hybrid electric propulsion, the fan would be driven with either a turbine engine or an electric motor. In turboelectric propulsion, the turbine engine and fan would be separated; the engine would drive a generator, and the electric motor would directly drive the fan. This would allow the fans to be distributed in a way that would decrease aircraft noise. Reducing the dependence on the turbine engine would certainly reduce emissions. However, the additional weight of the electric-motor-related components that would have to be added would reduce the benefits of the smaller turbine engine. Before this technology can be implemented, research needs to be done on improving component efficiencies and reducing component weights.

1.1 Background

Hybrid electric and turboelectric propulsion concepts must have high efficiencies in converting electrical power into usable thrust, comparable to those of the gas turbine engines that they will replace. The most powerful and efficient electric motors employ superconducting elements that must be operated at cryogenic temperatures. Although the benefits of cryogenic electric motors would appear to make them ideal candidates for electric propulsion, the cryogenic technology exacts a steep price in terms of the complexity and additional weight of the components required to maintain the extremely low temperature of the motor's superconductors. As an alternative, ambient temperature (noncryogenic) motors should become viable candidates for electric propulsion as expected technology improvements are made over the next few decades.

Figure 1 shows a schematic of a hybrid electric propulsion concept for aircraft (Ref. 1). Propulsion is provided by a fan,

which is either driven by the turbine engine or by an electric motor. Energy is provided to the motor through a transmission line from some kind of energy storage device, denoted as a battery pack. During cruise, the motor can drive the fan without the turbine engine, reducing emissions and fuel burn. The turbine engine also can drive the fan when extra power is needed, such as during takeoff.

For successful implementation of the hybrid electric propulsion system, there will need to be significant increases in the energy density and power density of the electrical components. The objective of this report is to (1) assess the state of the art for each of the electrical components, (2) project how future advances in technology can enable components with high power density and high energy density, and (3) project technology capabilities for electrical components in 15 and 30 years. This study is focused on electrical components for two cases: (1) eight-passenger aircraft and (2) single-aisle, 150-passenger aircraft.

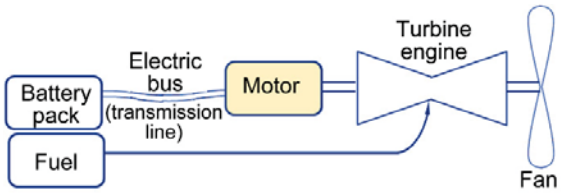

Figure 1.—Hybrid electric propulsion (Ref. 1).

The technology improvements being investigated in this study (Fig. 2) include motor-related technologies, power electronics, and energy-storage-related technologies. Motor efficiency and power density could be improved through the use of better conductors, insulators, magnets, bearings, structural materials, and thermal management. Energy storage could be accomplished through batteries, flywheels, or supercapacitors, all of which expect significant energy density improvements over the next few decades. Table 1 describes the types of improvements expected in each technology area over the years. Improvements will come from new high-performance, low-density materials and technologies, allowing increases in efficiency, power density, and energy density.

This report summarizes the results of a study performed at the NASA Glenn Research Center that assessed potential technology improvements for noncryogenic hybrid electric propulsion. The study was done under the NASA Subsonic Fixed Wing Project and was meant as a parallel path to complement the existing Cryogenic Hybrid Electric Program.

Cryogenic hybrid electric aircraft will require the development of new technologies throughout the aircraft system, including superconducting motors, generators, and transmission lines; cryogenic power electronics; and cooling (e.g., cryocoolers). These technologies will bring great efficiency benefits, but all of them are at a relatively low technology readiness level (TRL). This study was an attempt to determine the benefits of a hybrid electric aircraft that would not need cryogenic components, which are currently at low TRLs.

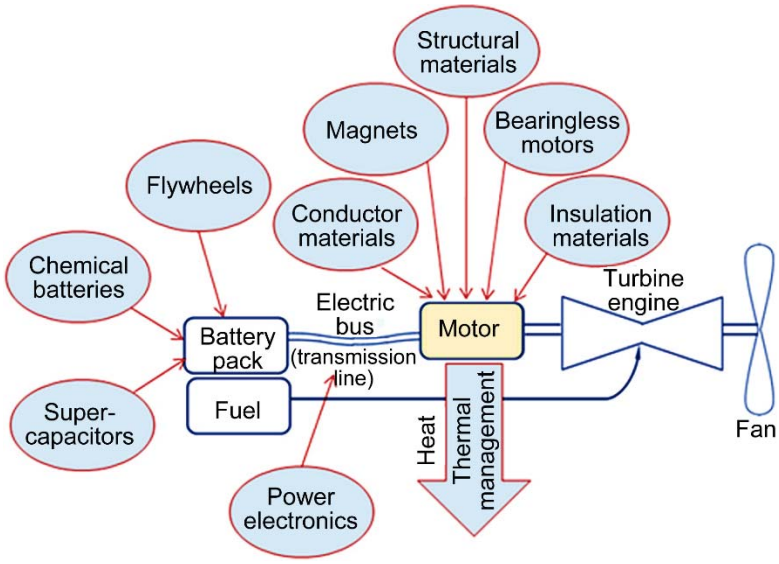

Figure 2.—Technology improvement areas for electric propulsion (based on Ref. 1).

TABLE 1.—MOTOR TECHNOLOGIES AND EXPECTED BENEFITS

Technology	Component	Component improvement	Benefits
Motor	Conductor material	Lower resistance and lower density materials	Reduced weight, reduced loss, and increased power
	Insulator material	Higher temperature and higher voltage capability Higher thermal conductivity	Higher power operation
	Permanent magnet material	Higher coercivity and remanent flux materials High-temperature magnet	Increased power
	Bearingless motor	Bearingless motor incorporates magnetic bearing within the motor, reducing the number of components	Reduced weight
	Structural materials	Higher specific strength materials	Decreased weight
	Thermal management	Lower density and higher thermally conductive materials	Increased efficiency and power density
Power electronics	Rectifiers and inverters	Improved switching components with high switching speed and topologies, improved filter components, new materials, and improved packaging	Increased efficiency and power density
Energy storage	Batteries	New battery chemistries	Higher energy density
	Supercapacitors	New supercapacitor chemistries	Higher energy density without sacrificing power density
	Flywheels	Higher specific strength materials allowing higher speed at lower weight	Higher energy density

TABLE 2.—SYSTEM REQUIREMENTS

Time from present, years	Electric motor power, MW	Motor voltage, V	Number of passengers	Power profile—portion of entire system power used, percent (Electric portion/fuel portion, percent)				
				Takeoff (5 min)	Climbout (30 min)	Cruise	Cruise duration, hours	Landing (5 min)
+15	1	700	8	100 (50/50)	90 (50/50)	50 (100/0)	2	100 (50/50)
+15	10	700	130	100 (50/50)	90 (50/50)	50 (100/0)	2	100 (50/50)
+30	1	1000	8	100 (50/50)	90 (50/50)	50 (100/0)	2	100 (50/50)
+30	10	1000	130	100 (50/50)	90 (50/50)	50 (100/0)	>2	100 (50/50)

1.2 Power Requirements

Table 2 summarizes the initial requirements for the study. On the basis of the analysis of requirements, this study considered improvements that were likely to be made by 15 and 30 years from now for 1- and 10-MW motors.

The power profile is based on zero emissions at cruise and the need for extra power in the event of a touch-and-go landing. The 700-V voltage limit was drawn from Reference 2. Beyond 700 V, thicker and costlier insulation is required, and insulation degradation due to partial discharge and corona becomes an issue. A system voltage of 1000 V, 30 years from now, assumes that technology improvements will allow the increase. The 2-h cruise is based on the 737 study (Ref. 3), which describes a 900-mi range at ~600 mph. Motor sizes of 1 and 10 MW were chosen as appropriate for use in the aircraft of interest. These motor power output classes were verified as described in the following paragraphs.

The Boeing 737–300 was used as an example to determine the required motor input power for a 150-passenger aircraft (Fig. 3). This was done to justify the consideration of the 10-MW motor as an alternative propulsor. The 737–300 was initially powered by two CFM56–3B–1 turbofan engines (Fig. 4) that each produced a maximum of 20 000 lbf of thrust. If the rule of thumb for turbofan engines is used that engine output horsepower is roughly equivalent to the thrust at rolling takeoff, and if it is assumed that each engine is producing maximum thrust at that moment, each CFM56 is thus producing 20 khp to drive its fan, or almost 15 MW. At takeoff, roughly 30 MW of mechanical power is being extracted from the fuel to accelerate this aircraft to flight. Under a main assumption of this study that the electric propulsion system must develop half of the required takeoff power, if two motors were used, each motor would have to produce 7.5 MW. Including the system losses adds to the required motor input power, so the total input power would be on the order of 10 MW. This validates the 10-MW motor output requested for this study for a 150-passenger vehicle.

Figure 3.—Boeing 737–300—an example of a 150-passenger aircraft (Ref. 4). Arpingstone grants anyone the right to use this work for any purpose, without any conditions, unless such conditions are required by law.

Figure 4.—CFM56–3 series turbofan engine found on the wings of the 737–300 (Ref. 5). Copyright 2005 GE Aviation; used with permission.

A similar study was performed for an eight-passenger aircraft, with the Learjet 25 used as an example (Fig. 5). The Learjet 25 uses two GE CJ610 turbojet engines, each of which produces a maximum of 3000 lbf of thrust (Ref. 7). Applying the same rule of thumb means that each engine generates approximately 3000 hp of output power. This is equivalent to 2.25 MW, for a total of 5 MW at takeoff. Half of this split between the two electric motors would be 1.13 MW, which is on the order of 1 MW. Considering motor system losses, this number would grow to at least 1.2 MW. This validates the assumption that an electric motor used to power an aircraft of this size might be on the order of 1 MW.

Figure 5.—Learjet 25—example of an eight-passenger aircraft (Ref. 6). Copyright Jetphotos.net; used with permission.

1.3 Assumptions

The following list summarizes the assumptions that the team used in this study:

(1) The aircraft is a hybrid electric or turboelectric aircraft. This assumption means that a portion of the propulsive power comes from fuel burn: that is, this is not an all-electric aircraft. Two basic configurations exist—the hybrid electric system and the turboelectric system.

(a) The turboelectric system converts the fuel burned to electricity via a turboshaft engine and a generator, which provides electrical power for electric motors that drive fans to produce thrust. In this case, almost all of the thrust comes from electric motors. Figures 6 and 7 show a concept for the electrical ducted fan and a schematic of the turboelectric propulsion system, respectively.

(b) The hybrid electric system combines the turbine engine and electric motor on one shaft (see the schematic in Fig. 1). Thus, propulsion comes directly from fuel and electrical power.

(2) There will be no emissions at cruise (per the requirements in Table 2).

(3) The “electric motor power” is the output of one motor.

(4) The vehicle configuration is left to the vehicle designers. This study addressed the motor and energy-storage aspects of the vehicle. The configuration of the vehicle (e.g., turboelectric vs. hybrid, or number of engines per plane) was left to the vehicle designer and was beyond the scope of this study.

(5) The energy storage systems considered in this study were batteries, flywheels, and supercapacitors.

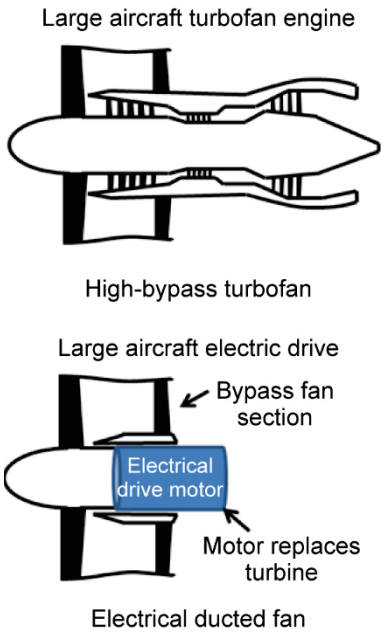

Figure 6.—Electrical ducted fan.

2.0 Motors

Permanent magnet (PM) motors were addressed specifically in this study because they are an attractive design for scaling to aircraft powers. The motor provides "free" flux from the PM; that is, unlike other motor types, PM motors do not need electric power to generate the flux. Also, they can be more power dense than their induction machine counterparts, they are quieter, and they include a smoother rotor, which provides windage and structural benefits. In addition, a bearingless configuration (which could be adapted to multiple electric motor types) was considered because of the potential benefits in terms of robustness, redundancy, and power density—allowing the lubrication system to be eliminated. However, because every electric motor type includes most of the key components considered in this study, the improved technologies identified would provide benefits for any motor type used in a hybrid electric aircraft.

Figure 8 shows the continuous power densities of some selected motors. There are several ways to define power density, depending on the power definition and the motor mass used. Sometimes the "active mass"—only the rotor and stator, without the housing—is used; this results in a higher power density. For this study, the total mass—rotor, stator, and housing—were used for the power density calculation, along with the continuous power, rather than the peak power. As we look to increase power density, we also will be targeting reducing the weight of the housing and support structure. For industrial megawatt-size motors, the power density is ~0.1 hp/lb. Several design studies for megawatt-class motors in support of U.S. Navy electric propulsion have proposed viable

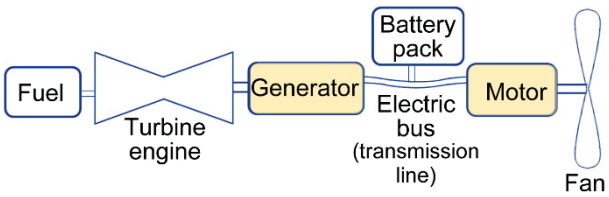

Figure 7.—Turboelectric propulsion system (Ref. 1).

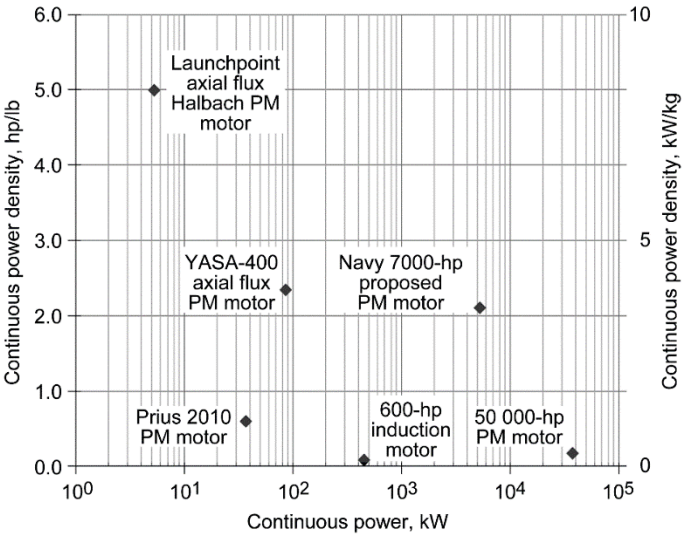

Figure 8.—Continuous power density of selected motors (data from Refs. 8 to 12).

designs with power densities on the order of 2 hp/lb. If a power density of 3 hp/lb is achieved, a 1-MW (1340-hp) motor should weigh approximately 215 kg (470 lb). The state-of-the-art power density for kilowatt-size motors is increasing steadily because of the technology need for hybrid-electric and all-electric automobiles. Hybrid vehicle motors can achieve ~1 hp/lb, and a new 5-kW axial-flux Halbach PM motor manufactured by LaunchPoint has achieved 5 hp/lb. In addition, many improvements could be made to the motor to improve both its power density and its efficiency, making it a more viable candidate for part of an aircraft propulsion system.

Electric motor components include the copper conductor that carries the electric current, the wire insulation, PMs in certain motor types, a composite wrap containing the rotating PMs, the bearings for the motor rotor, and the motor housing and structural support. Electric motors heat up during use, degrading efficiency and power. Also, the power electronics needed to convert power and drive the motor add more weight to the system.

The power density of the motor can be increased by (1) increasing power output, (2) decreasing weight, and/or (3) increasing the power density of the power electronics. The power output P of a motor is governed by the relation (Ref. 13):

$$P = k\eta ABd^2LN \tag{1}$$

where k is a factor that includes geometrical and electrical information, η is the efficiency, A is surface current density, B is the air-gap flux density, d is the air-gap surface diameter, L is the stator core length, and N is the rotational speed. The surface current density and air-gap flux density can be increased by incorporating advanced electromagnetic designs, increasing the strength of the magnets, increasing the electrical conductivity of the conductors, improving thermal management techniques for keeping the component temperatures within their operating limits, and increasing the temperature capability of various components (e.g., magnets and electrical insulation materials). The weight of the motor can be decreased by introducing lightweight, high-strength materials and advanced structural concepts.

The conductors used in motors today are typically copper. Although copper is highly conductive, its conductivity decreases with temperature and it is quite heavy. Future improvements are expected in new materials with high conductivity, low resistivity, and low density.

In addition, the wire is surrounded by an electrically insulating material. This material has limits in terms of voltage capacity, maximum temperature, and thickness. The motors for electric propulsion are expected to run at very high voltages and higher temperatures, and it will be important to develop new insulation materials to handle this extreme environment. The insulation should also have high thermal conductivity, improving heat transfer within the motor.

The strongest PMs today are made of neodymium-iron-boron (NdFeB) or samarium-cobalt (SmCo)—materials that have high coercivity and high remanent flux. However, new magnet materials are being developed with even better properties, which would improve the power density of the motor.

In the future, the bearings required to suspend the motor rotor might be active magnetic bearings. If the magnetic bearing function is made part of the motor design itself, such as in a bearingless motor, component weight will decrease.

During operation, the motor will heat up because of I^2R losses within the conductor (where I is current and R is resistance). Increasing temperature has a negative effect on the conductor's resistivity, the insulation properties, and the magnet strength. Although incorporating thermal management into the motor system would improve the motor's efficiency, a heat exchanger would add weight to the motor system, decreasing its power density. New materials that are being developed with high thermal conductivity and low density could be used as part of a heat exchanger that would help improve the motor's efficiency without adding significant weight.

This type of aircraft propulsion system will require power electronics to convert power and to drive motors. Significant improvements are possible to state-of-the-art power electronics, including components, switch and filter materials, switching topologies, and packaging.

The following sections give detailed explanations of the predicted improvements in these motor components and technologies along with the benefits expected.

2.1 Conductors With High Electrical Conductivity

Copper is the most widely used electrical coil material used today for electric motors. Superconducting materials have significantly higher electrical conductivity than copper. However, the best high-temperature superconducting materials, such as yttrium barium copper oxide (YBaCuO) compounds and magnesium diboride (MgB_2), require cryogenic temperatures: YBaCuO requires cryogenic temperatures corresponding to liquid nitrogen, and MgB_2 requires temperatures corresponding to liquid hydrogen. However, cryogenic technology exacts a steep price in terms of the complexity and weight of the containment vessel for the cryogen required to maintain the extremely low temperature of the motor's superconductors. This weight/complexity problem must be surmounted before cryogenic propulsors can be integrated into future aircraft. Room temperature conductors with significantly higher electrical conductivity than copper would be preferred. One type of candidate, nanoconductors, are fabricated from carbon nanotubes (CNTs). CNTs hold the promise of creating nanoconductors that would have substantially higher conductivity at room temperature and lower weight than copper or any of its alternatives (such as aluminum).

2.1.1 State of the Art of Carbon Nanotube Conductors

CNTs are members of the fullerene structural family—that is, Buckminsterfullerene (buckyball), which is a form of carbon. Other forms of carbon include diamond, graphite, lonsdaleite, and amorphous carbon. CNTs have cylindrical structures, with typical examples shown in Figure 9 (Ref. 14). These structures

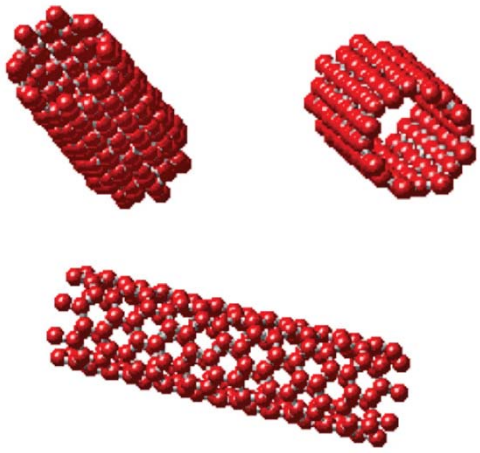

Figure 9.—Single-wall carbon nanotube in various orientations (Ref. 14). Copyright Vincent Crespi, Dept. of Physics, Pennsylvania State University; used with permission.

usually exhibit a length-to-diameter ratio of 132 000 000:1, and they also have unusual properties, which make them valuable to the fields of optics, material science, and electronics (Ref. 15). CNTs have been fashioned in lengths ranging from the shortest, observed in the organic compound cycloparaphenylene, which was synthesized in 2009, to the longest (18.5 cm long), which also was produced in 2009 (Ref. 15). They also vary in diameter from about 3 to 30 nm (30 to 300 Å) (Ref. 16). These tubes exhibit very high thermal conductivity, comparable to that of diamond, and they are the strongest and stiffest materials discovered to date, with tensile strengths on the order of 63 GPa. This tensile property was demonstrated in 2000, and a 2008 study revealed strengths of about 100 GPa (Refs. 15 and 17).

Our interest in this material lies in its electrical properties. The symmetrical arrangement of the carbon atoms of graphene (the building blocks of CNTs) (Ref. 18), coupled with its unique electronic structure, have sparked interest in this material as an alternative to copper and aluminum with its wire variant, known as copper-clad aluminum (Ref. 19). Depending on their crystal lattice structure, CNTs can be either metallic conducting or semiconducting. In their conducting mode, CNTs exhibit current densities on the order 4×10^{9} A/cm^2: 1000 times that of copper (Ref. 15). Clearly, fashioning this material into a conductor could bring us closer to the goal of room temperature superconductivity, without the complexity and weight of cryogenic technology. The density of solid CNT material is on the order 1.3 to 1.4 g/cm^3 (Ref. 15), compared with copper's 8.96 g/cm^3 (Ref. 20). Using CNTs will result in an 84-percent reduction in weight relative to copper. In addition, CNT conductivity does not decrease with temperature as it does with copper. Obviously, the superior conductivity and weight savings in employing nanoconductor wiring in aircraft and in electric motor coils will substantially improve fuel burn efficiencies. The properties just described apply to random, nonaligned nanotubes. The goal now is to fabricate a wire conductor by effectively connecting individual nanotubes into one continuous strand that has the same desirable properties as its individual components. Fabricating nanoconductors is a rather difficult and complex task, which elevates the cost of the wires. Overcoming these challenges is a critical step on the path to replacing copper conductors with nanoconductors.

The nanoconductors fabricated thus far have much higher resistivity than copper or aluminum. One theory suggests that electrons flow unimpeded through individual nanotubes (superconductivity on a nanoscale) but experience difficulty crossing the boundary between connected tubes, thus contributing to the higher resistivity observed in nanoconductors. Because of the significant hurdles presented by nanoconductor fabrication, only a handful of companies and universities have taken up the challenge of producing nanoconductors. A few years ago, General Nano, LLC (Ref. 21), in partnership with Glenn, proposed building an electric motor wherein the copper wire would be replaced with CNT "thread electrical fiber." In addition, Nanocomp Technologies, Inc. (Ref. 22), incorporated in 2004, has a commercial production facility that manufactures CNT sheets and cables Figs. 10 and 11). The nanoconductor currently produced by Nanocomp has a resistivity 234 times that of copper.

In 2011, Rice University (Ref. 23) reported producing double-walled nanotubes that were doped with iodine and subsequently fashioned into cables having resistivity of 1.5×10^{-7} Ω-m. This is approximately 9 times more resistive than oxygen-free copper at 1.68×10^{-8} Ω-m. The specific conductivity of this material is 71 percent that of copper, which could make it a viable alternative to copper for transmission lines in the near future. However, motor coils have limited space, so the nanoconductor will need an absolute resistivity closer to that of copper to see power density benefits. Behabtu shows that the specific conductivity of the nanoconductors is about an order of magnitude higher than that of copper (Ref. 24). Clearly, this trend is advancing in the right direction, and nanoconductors significantly more conductive than copper could become a reality in 15 years and enjoy widespread application in 30 years.

Figure 10.—Nanocomp large conductors (Ref. 22).
Courtesy of Nanocomp Technologies, Inc.

Figure 11.—Nanocomp large sheet capability (Ref. 22).
Courtesy of Nanocomp Technologies, Inc.

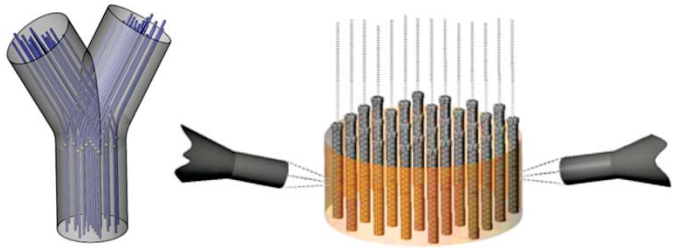

Figure 12.—Nanotubes embedded in metal cladding (Ref. 25). (Unless otherwise indicated, this information has been authored by an employee or employees of the Los Alamos National Security, LLC (LANS), operator of the Los Alamos National Laboratory under Contract No. DE-AC52-06NA25396 with the U.S. Department of Energy. The U.S. Government has rights to use, reproduce, and distribute this information. The public may copy and use this information without charge, provided that this Notice and any statement of authorship are reproduced on all copies. Neither the Government nor LANS makes any warranty, express or implied, or assumes any liability or responsibility for the use of this information.)

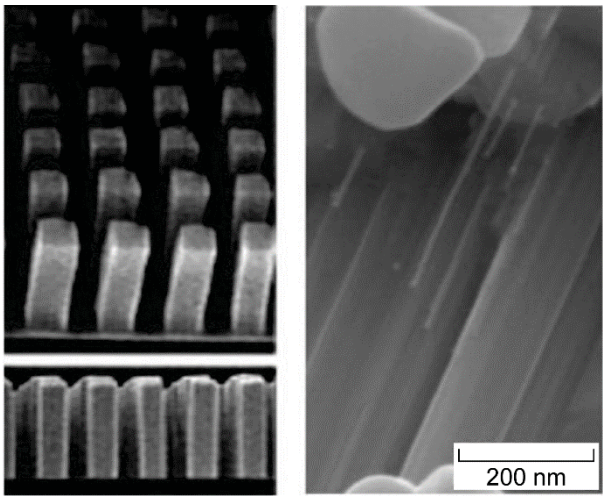

Figure 13.—Carbon nanotube microstructure using the "Ultraconductus" process (Ref. 25). (Unless otherwise indicated, this information has been authored by an employee or employees of the Los Alamos National Security, LLC (LANS), operator of the Los Alamos National Laboratory under Contract No. DE-AC52-06NA25396 with the U.S. Department of Energy. The U.S. Government has rights to use, reproduce, and distribute this information. The public may copy and use this information without charge, provided that this Notice and any statement of authorship are reproduced on all copies. Neither the Government nor LANS makes any warranty, express or implied, or assumes any liability or responsibility for the use of this information.)

Another promising conductor technology uses the Ultraconductus process developed at Los Alamos National Laboratory (Figs. 12 to 14 and Ref. 25). Aligned CNTs, approximately 10 nm in diameter, are embedded in a metal cladding (a process involving laser ablation). This ensures conduction horizontally between tubes. There is very little resistance along the length of the nanotubes (i.e., they are ballistic or quantum conductors). Unlike copper, the ultraconductor electrical conductivity does not decrease with temperature.

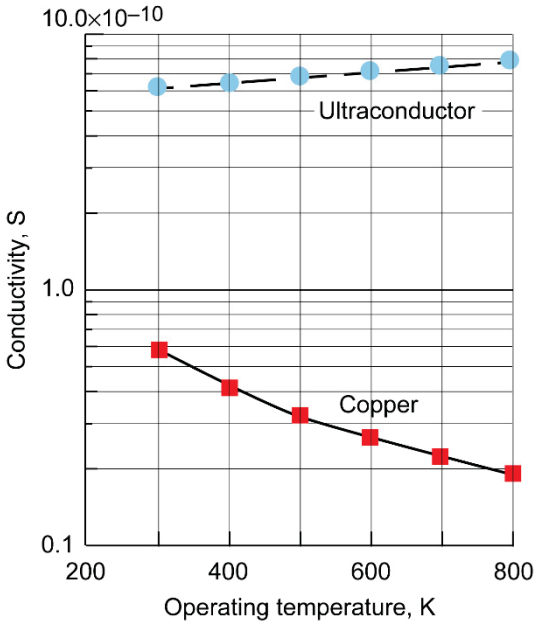

Figure 14.—Electrical conductivity of ultraconductor versus copper (Ref. 25). (Unless otherwise indicated, this information has been authored by an employee or employees of the Los Alamos National Security, LLC (LANS), operator of the Los Alamos National Laboratory under Contract No. DE-AC52-06NA25396 with the U.S. Department of Energy. The U.S. Government has rights to use, reproduce, and distribute this information. The public may copy and use this information without charge, provided that this Notice and any statement of authorship are reproduced on all copies. Neither the Government nor LANS makes any warranty, express or implied, or assumes any liability or responsibility for the use of this information.)

TABLE 3.—CONDUCTOR BENEFITS SUMMARY

Nanoconductor characteristics	State of the art	+15 years	+30 years
Reduction in weight (CNT/copper), percent	~16	~16	~16
Increase in resistivity (CNT/copper)	9 × Cu	1 × Cu	0.5 × Cu
Increase in power loss (CNT/copper), percent	900	100	50
Improvement in horsepower per pound (CNT/copper), percent	–87 to –81	20 to 72	140 to 245

2.1.2 Possible Improvements to the Electrical Conductivity of Carbon Nanotube Conductors

To improve the electrical conductivity of CNTs, researchers may target lengthening the nanotubes (reducing the number of boundaries between nanotubes), improving the conductivity among shorter nanotubes, or finding a way to separate the conductive and nonconductive nanotubes. In light of the technical challenges, Table 3 shows a projection of the advancement of CNT conductor characteristics 15 and 30 years from now. By 15 years, one can expect an 84-percent reduction in conductor weight, with a simultaneous decrease in resistivity to where it is on par with that of copper, and by 30 years, a decrease in resistivity to half that of copper conductor. A 50-percent further decrease in resistivity would mean that the conductor could carry twice the current load at a given voltage while simultaneously cutting power losses in half. With significant increases in the electrical conductivity of CNTs, CNT-reinforced copper composites will also be potential candidates to replace copper for the conducting coil in motors.

2.1.3 System Benefits of Nanoconductor Improvements

The power density benefits shown in Table 3 assume a copper weight of 20 to 50 percent of the motor's active weight. The actual amount will depend on the motor type.

2.1.4 Path Forward for Carbon Nanotube Conductors

Our projection is that CNT-based fibers will have electrical conductivity equal to or better than that of copper. However, breakthroughs in CNT synthesis and fiber fabrication processes could result in a significant increase in electrical conductivity much earlier than 30 years. In the meantime, research effort should be focused on building electrical motors with available CNT fibers so that challenges related to the development of nanotube-conductor-based electric motors can be identified much earlier.

2.2 Wire Insulation

The power of a given motor configuration is limited by the allowable current within the conductor. This current is, in turn, limited by the temperature capability of the wire insulation. Motor wire insulation is specified by maximum temperature, for example, 105 °C for plain enamel and 240 °C for polyimide insulation (Ref. 26). Increasing the high-temperature capability will enable operation with a higher current, increasing the power density of the motor.

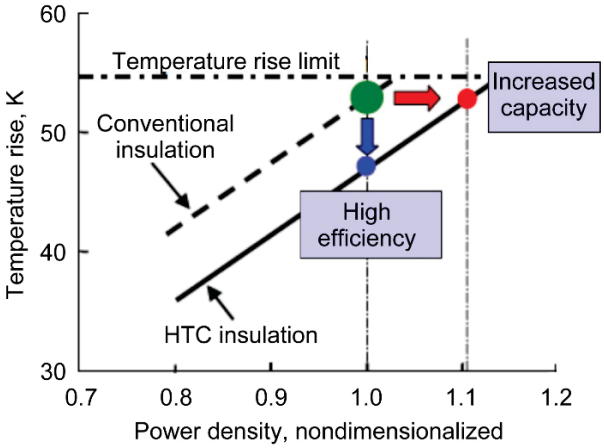

Figure 15.—Effect of high-temperature-conducting (HTC) insulation on power density of a turbine generator (Ref. 27). Copyright Institute of Electrical Engineers of Japan; used with permission.

A stator coil will have insulation surrounding each wire strand and insulation around each turn, in addition to groundwall insulation. This buildup of insulation typically allows for very low thermal conduction from the wires to the surroundings. Increasing the thermal conductivity of the insulation materials will decrease the temperature within the conductor, allowing for operation with a higher current. Again, this will enable an increase in the power density of the motor.

Figure 15 illustrates the effect of temperature rise on the power density of an electric machine. This particular case is a 600-MVA-class turbine generator that is indirectly cooled by hydrogen. It shows the impact of doubling the thermal conductivity of the stator coil insulation, allowing a 10 percent increase in power density or increased efficiency for the same power density (Ref. 27).

Another challenge for the wire insulation used in hybrid electric propulsion is the expected higher voltage: 700 to 1000 V (see Table 2). This has implications for both the motor wire and the transmission cables. Paschen's Law states that the breakdown voltage of air is much lower at the low pressure levels at aircraft cruise altitudes, approaching a minimum at less than 400 V. Transmission cables especially need to use high-voltage insulation because they can have the full high-voltage difference between cables. Motor coils will also see higher

voltage between turns or windings, although not the full 700 to 1000 V. In addition, electrical surges may occur, for example from the inverter (Fig. 16, from Kikuchi and Hanawa, Ref. 28). To accommodate high voltage within an aircraft, the insulation material must have high dielectric strength. Corona discharge often produces pin holes, degrading the insulation. Employing a proper insulation material will minimize not only corona discharge but also arcing between wiring or adjacent components. The dielectric breakdown strength is typically given in units like kilovolts per millimeter; hence, better insulating materials might also result in thinner insulation. This would reduce the size of the motor windings and potentially the motor weight, thereby increasing the power density.

In addition to improved thermal and voltage properties, the wire insulation must have the strength and flexibility to enable it to be wound into a coil, must be thin enough to make the coil compact, and must be compatible with the substances in the environment and other substances used in the motor coil (e.g., varnish).

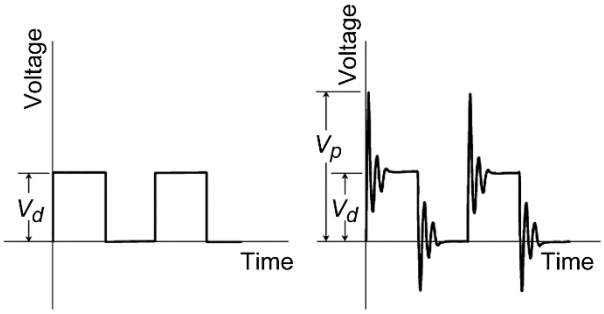

Figure 16.—Typical terminal voltage waveform (Ref. 28), where V_d is the drive voltage and V_p is the peak voltage. (a) Voltage at inverter terminal. (b) Voltage at motor terminal. © 2012 IEEE. Reprinted, with permission, Kikuchi, Hideyuki; and Hanawa, Hidehito: Inverter Surge Resistant Enameled Wire With Nanocomposite Insulating Material. IEEE Trans. Dielec. Elect. Insul., vol. 19, no 1, 2012, pp. 99–106.

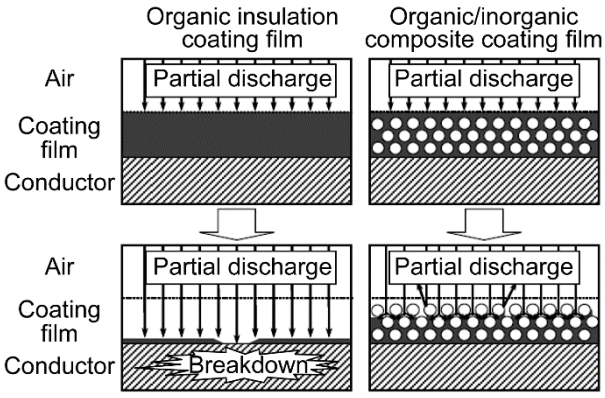

Figure 17.—Mechanism of erosion suppression (Ref. 28). © 2012 IEEE. Reprinted, with permission, Kikuchi, Hideyuki; and Hanawa, Hidehito: Inverter Surge Resistant Enameled Wire With Nanocomposite Insulating Material. IEEE Trans. Dielec. Elect. Insul., vol. 19, no 1, 2012, pp. 99–106.

2.2.1 State of the Art of Wire Insulation

Motor wire (also known as magnet wire) is defined by diameter, temperature class, and breakdown voltage. The insulation defines the temperature class and breakdown voltage, in addition to the application environment. The insulation can be built of several layers, depending on the required properties.

A typical high-temperature wire insulation is polyimide, which has a 240 °C maximum temperature. This material also has a relatively high dielectric breakdown strength, on the order of 200 kV/mm (Ref. 29). However, the thermal conductivity of wire insulation is fairly low, for example on the order of 0.01 to 0.1 W/mK (Refs. 29 and 30) compared with 400 W/mK for the copper conductor.

Polyetheretherketone (PEEK), another high-temperature wire insulator, has a maximum operating temperature of 260 °C (Ref. 31). Its dielectric strength—about 20 kV/mm—is lower than that of polyimide, and its thermal conductivity—0.25 W/mK—is higher (Ref. 32).

To improve the thermal and voltage capability of magnet wires, extra layers of insulation can be added with special materials, or fillers can be added to the insulation. For example, a heat-resistant wire has been developed that uses nanosized silica particles dispersed within the polyimide insulation layer over a nickel-plated copper conductor (Ref. 33). This material increases the temperature capability from 240 to 280 °C and reduces the breakdown voltage of the wire from 12.0 kV to about 9.8 kV. However, it is better able to sustain the breakdown voltage over a longer period of time. Another wire insulation configuration was constructed specifically to improve discharge resistance. The researchers suggest that the added silica nanoparticles extend the path through which the charged particles must travel, which suppresses breakdown (see Fig. 17 from Ref. 28).

2.2.2 Possible Improvements to Wire Insulation

Boron nitride (BN) is one compound that potentially could be used as an insulator. BN has good thermal stability and conductivity and good electrical resistance properties. However, there are some immediate challenges that must be overcome before BN can be a viable insulator. One key challenge is effectively dispersing BN nanotubes (BNNTs) in an appropriate polymer, which would then be used to coat the conductor. This technique has not yet been perfected. Apparently it is difficult to disperse BNNTs within polymers without affecting mechanical properties.

BNNTs that were synthesized and tested at Glenn showed excellent thermal stability (Fig. 18) and had a high electrical bandgap of 5.5 eV. In theory, single-walled BNNTs can have a thermal conductivity of 3000 W/mK; however, in practice this value is lower. Currently, a thermal conductivity of 200 to 300 W/mK can be expected from a BNNT with an approximate diameter of 40 nm (Ref. 34).

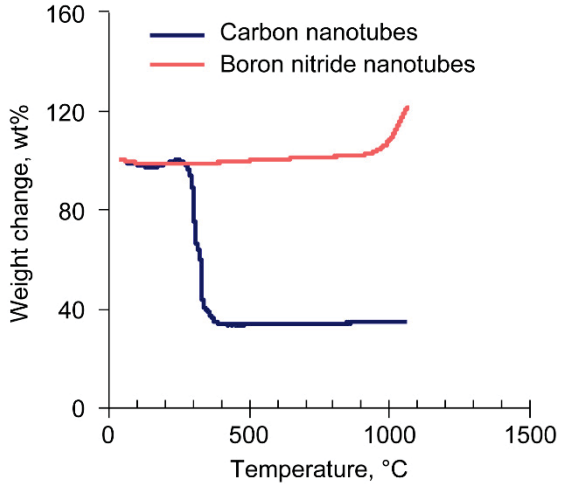

Figure 18.—Weight change of carbon nanotubes (CNTs) and boron nitride nanotubes (BNNTs) in air.

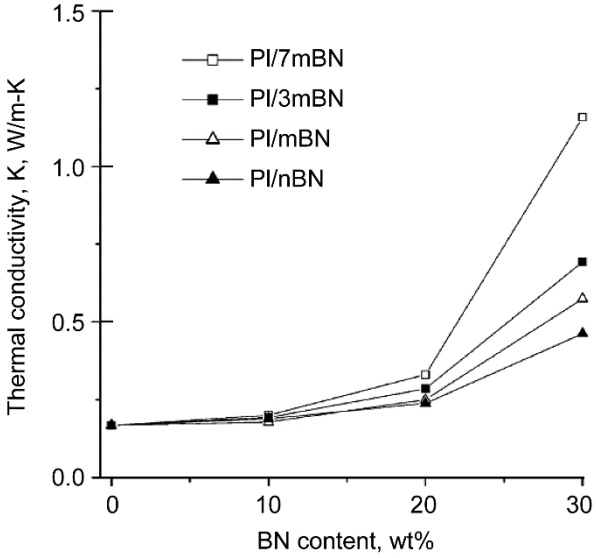

Figure 19.—Thermal conductivity of polyimide/boron nitride (PI/BN) composite films with different BN contents (Ref. 35), where *m* and *n* refer to different BN sizes and ratios. Reprinted with permission from Li, Tung-L.; and Hsu, Steve Lien-Chung: Enhanced Thermal Conductivity of Polyimide Films Via a Hybrid of Micro- and Nano-Sized Boron Nitride. J. Phys. Chem. B, vol. 114, 2010, pp. 6825–6829. Copyright 2010 American Chemical Society.

TABLE 4.—INSULATION IMPROVEMENT FORECAST SUMMARY

Insulation characteristics	+15 year	+30 year
Thermal conductivity increase	10 times	20 times
Insulation thickness decrease, percent	50	75
Power density increase, percent	25	40

Before BNNTs can be utilized in magnet wire insulation, research needs to be performed in the manufacture of the composite insulation. Zhi et al. (Ref. 34) show that dispersing BNNTs within certain polymers can increase their thermal conductivity to as high as 3.6 W/mK, a twentyfold increase over the baseline. Coil insulation will more likely be fabricated of something like polyimide. Li and Hsu (Ref. 35) fabricated thermally conductive polyimide film with up to 30 wt% microsized and nanosized BN. Figure 19 shows their results for thermal conductivity of the composite material as a function of BN content. The highest thermal conductivity resulted from a combination of 70 wt% microsized BN and 30 wt% nanosized BN, yielding almost an order of magnitude increase in thermal conductivity versus the baseline polyimide material.

2.2.3 Summary of Wire Insulation Findings

Although researchers are exploring the use of BNNTs as part of electrical insulation, challenges remain in the implementation. It is quite possible that in 15 years BNNT composite insulation that has 10 times greater thermal conductivity and 50 percent thinner insulation will be widely available. We hope that, in 30 years, thermal conductivity will increase 20 times and insulation thickness will decrease by 75 percent. These advances should allow for a 25-percent increase in power density in 15 years and a 40-percent increase in 30 years (see Table 4).

2.3 Permanent Magnets

The noncryogenic motors used to drive fans in commercial transport aircraft will likely contain PMs. Brushless, synchronous, and toothless PM motors can have smooth rotors, potentially larger air gaps, and lower losses than other motor types. NdFeB magnets will be used unless temperature requirements call for SmCo magnets, which maintain their magnetization at higher temperatures but are not as strong as NdFeB magnets (Ref. 36).

PMs can be purchased in different shapes and sizes. Their cost depends on their rare earth material content, fabrication method, and value of $(BH)_{max}$, the maximum product of the magnet's remanence B_r and its coercivity H_c. Essentially, $(BH)_{max}$ determines a magnet's strength: the higher the number, the stronger the magnet. Figure 20 compares the sizes of magnets with different energy products required to achieve a flux density of 1000 G at 5 mm from the pole surface (Ref. 37). The number in the name of each magnet is its energy product value. As *BH* increases, the required size of the magnet decreases. Benefits of higher *BH* include lighter weight actuators and lower circuit leakage, which lead to higher power density and greater efficiency, respectively.

Reference 38 details the historical development of several types of PMs, showing that NdFeB, despite its relatively recent discovery in 1982, is much stronger than its predecessors and is the state of the art.

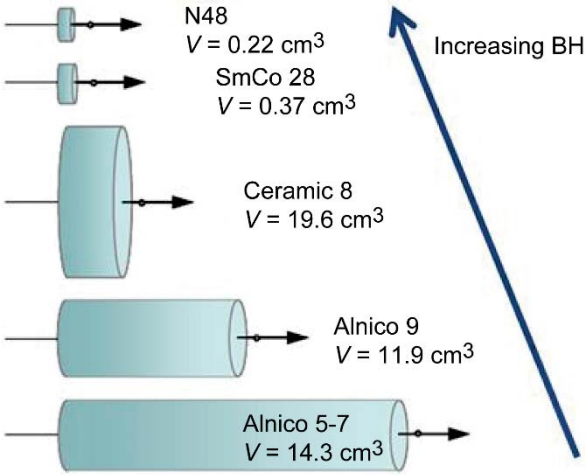

Figure 20.—Relative magnet size and shape to generate 1000 G at 5 mm from the pole surface (Ref. 37). Alnico is an alloy primarily consisting of Al, Ni, and Co; SmCo, samarium cobalt; *V*, volume; *BH*, energy product. Copyright 2010 Arnold Magnetic Technologies Corp.; used with permission.

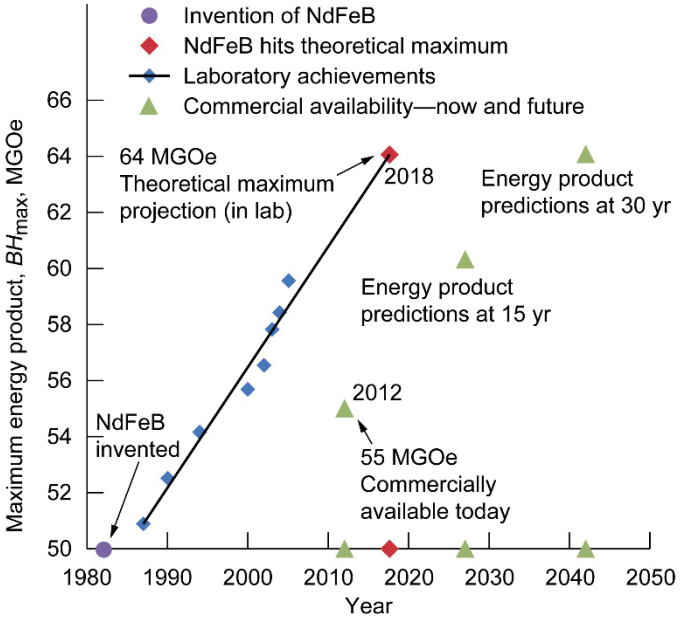

Figure 21.—History and predictions of energy product improvements for neodymium iron boride (NdFeB) sintered permanent magnets.

2.3.1 State of the Art of Permanent Magnets

Currently, NdFeB magnets can be purchased with energy products up to 55 MGOe (Ref. 39). NEOmax offers a PM with this capability. The theoretical limit for the energy product of an NdFeB magnet is 64 MGOe, and it is likely that a magnet with this energy product will be available by 2042. In 2005, NEOmax achieved, in its laboratory, the current record for energy product—59.5 MGOe (Ref. 40). However, magnets with this much energy are not yet available commercially. Figure 21 presents the NdFeB PM data graphically. The demand for these magnets has increased significantly since their discovery. In 1991, 1200 metric tons of NdFeB were produced in Japan. In 2004, 7200 tons were produced (Ref. 40). As demand has increased, so too has the level of research toward improving the capabilities of these magnets, which will facilitate continued improvements in this class of PM.

2.3.2 Possible Improvements to the Properties of Permanent Magnets

Figure 21 shows a history of NdFeB laboratory energy product advances as well as predictions for commercially available product. It is reasonable to anticipate that NdFeB magnets with an energy product greater than 58 MGOe will be available by 2027. By 2042, NdFeB magnets likely will approach their full potential of 64 MGOe. Figure 22 shows predicted future values of remanence B_r and coercivity H_c for NdFeB at 15 and 30 years out. The upper bound of 1.65 T for B_r by 2042 is 10 percent higher than that for magnets available today.

Different processing techniques and chemical constructs will facilitate the tailoring of the remanence and coercivity for applications where one or the other is more important. For noncryogenic motors designed for hybrid aircraft propulsion, both remanence and coercivity will be important. For candidate motors like LaunchPoint's Halbach motor (Ref. 41), the higher the remanence, the better. Motor air-gap flux is related to B_r. The output power of motors of this type are directly proportional to B_r, at least in simple one-dimensional analyses. The coercivity of the magnet is important because, when placed in close proximity to motor coils, these magnets could demagnetize if the local coil's magnetic field ever spiked high enough. Higher coercivity means a higher energy product, which in turn means that the magnet will be less susceptible to demagnetization.

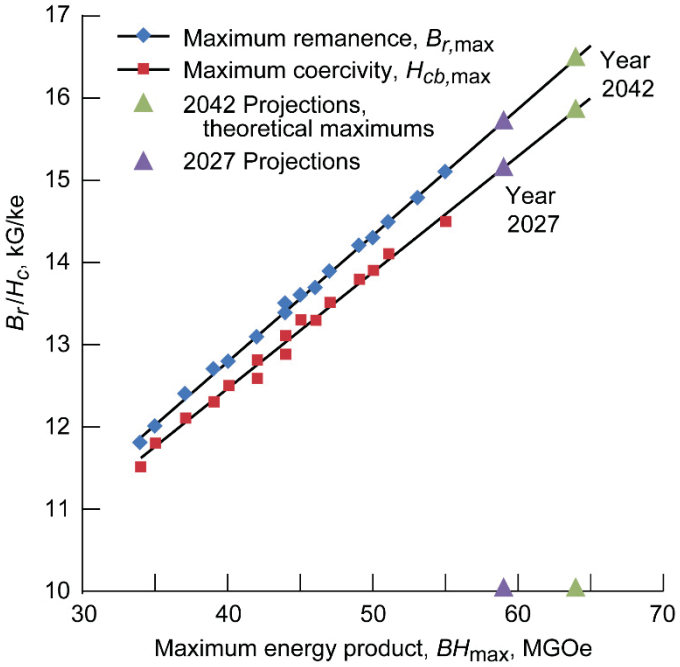

Figure 22.—NdFeB permanent magnet B_r and H_c versus energy product; data extracted from product sheets in Reference 39.

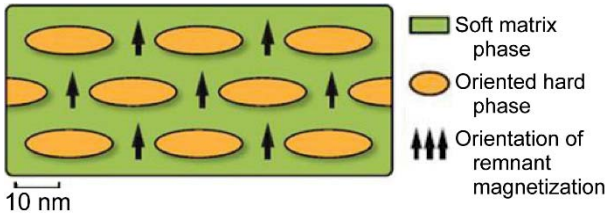

Figure 23.—GE construction of finely tuned molecular-scale permanent magnets (Ref. 38). Copyright 2013 GE Global Research; used with permission.

In Reference 42, an energy product of 137 MGOe is claimed to be achievable in a PM when an approach is used that involves clever exchange hardening in nanoscale combinations of alternating soft and oriented hard magnetic material phases. The 137-MGOe energy product is more than double what is theoretically possible with NdFeB magnets. PMs of this type will contain a much smaller percentage of rare earth elements and more iron (Refs. 42 to 44).

Coey and Skomski (Ref. 42) also suggest that a PM with a remanence of over 2.0 T should be achievable. In addition, it may not be outside the realm of possibility that a PM could be constructed that can maintain a remanence of 2.4 T, which is the saturation level of soft magnetic alloys like Hyperco 50.

The Department of Energy has funded academia and industry to develop new improved magnets. The main drive of the effort is to build magnets up on a molecular level using much less rare-earth-element content. Rare earth elements are expensive and are not readily found domestically. The United States depends exclusively on foreign sources of these materials. This puts the U.S. economy and energy security at risk. Because these new magnets will contain up to 80 percent less rare earths (like neodymium and samarium) and more readily available iron, they should be cheaper.

Both GE Global Research (Ref. 43) and the University of Delaware (Ref. 44) were recently funded to develop the techniques to fabricate such magnets. Their predicted performance numbers are eye opening. These magnets would revolutionize more than just motors. GE and the University of Delaware are working under Department of Energy funding to develop new magnets that would be more powerful than NdFeB magnets and commercially available by 2027. Clever pinning of magnetic moments using nanoscale material particles and three-dimensional arrangement techniques could potentially take the value of remanent flux density to levels typically found in soft magnetic materials such as Hyperco. Hyperco (not a PM) has a saturation flux density of 2.4 T. This is 63 percent higher than the remanent flux density of NdFeB magnets currently available today. For a machine such as LaunchPoint's ironless Halbach motor (Ref. 41), this could result in an increase in power density of at least 63 percent (based on a simple one-dimensional analysis) because of PM improvements alone. There could be additional benefits due to an increase in coercivity. Most increases in magnet energy product today are due to higher coercivity H_c and not remanent flux density B_r. This is because, in today's PMs like NdFeB, B_r is already close to theoretical spontaneous magnetization limits (Ref. 42). Higher coercivity will allow for the consideration of windings that produce higher alternating current (AC) in a given motor design. Higher coercivity, coupled with a higher magnet Curie temperature, also makes a PM less susceptible to demagnetization at elevated temperatures. Coupled with new conductors, insulators, and advanced thermal management techniques, improved NdFeB magnets and future nanocomposite magnets will undoubtedly help push motor power densities higher.

The devil, of course, lies in the details of just how to fabricate these new magnets from molecular-sized pieces. In both projects, soft and hard magnet nanosized building blocks are to be arranged in optimum three-dimensional ways to orient and pin magnetic moments to achieve very high remanent flux densities as well as more coercivity than is typical.

Figure 23 provides GE's basic composite magnet layout with alternating soft and hard magnetic nanoparticles (Ref. 38). The hard-phase material orients the field in the soft material and holds it.

Researchers at the University of Delaware also are utilizing both soft and hard materials (Ref. 44). The university plans to use material preparation techniques such as wet chemistry or ball milling to make the nanoparticles prior to using an unmentioned technique to assemble them into a magnet. A doubling of energy product is predicted.

Figure 24 graphically shows why using smaller building blocks of hard and soft material creates a better magnet (Ref. 45). In Figure 24(a), the lower blue material is hard (NdFeB) and the upper white material is soft (iron). The arrows represent the direction of the magnetic field within the material. Notice that the arrows in the hard material stay fixed, pointing to the left over the span. In the soft material, the arrows are aligned with those in the hard material at the boundary between materials. But as the distance from the boundary increases, the arrows become less oriented. The hard material aligns the direction of the field within the soft material at the boundary, but the influence decays. This shows that the smaller the vertical span of the soft layer is, the better aligned the field will be throughout it. This gives credence to assembly of these materials with small particles.

Figure 25 shows the predicted improvements expected from these new nanocomposite magnets (Ref. 46). Use of nanocomposites can almost double the maximum energy product $(BH)_{max}$.

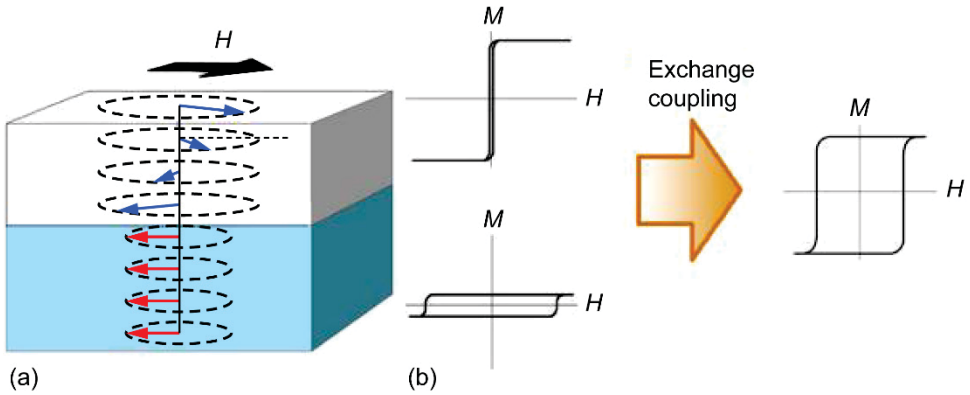

Figure 24.—Graphical explanation of exchange coupling showing improved PM energy product through the combination of hard and soft materials (Ref. 45). (a) Magnetic field in hard (lower portion) and soft (upper portion) materials. (b) Exchange coupling of hard and soft materials. *H*, magnetic field; *M*, magnetization. Copyright 2008 George Hadjipanayis, University of Delaware; used with permission.

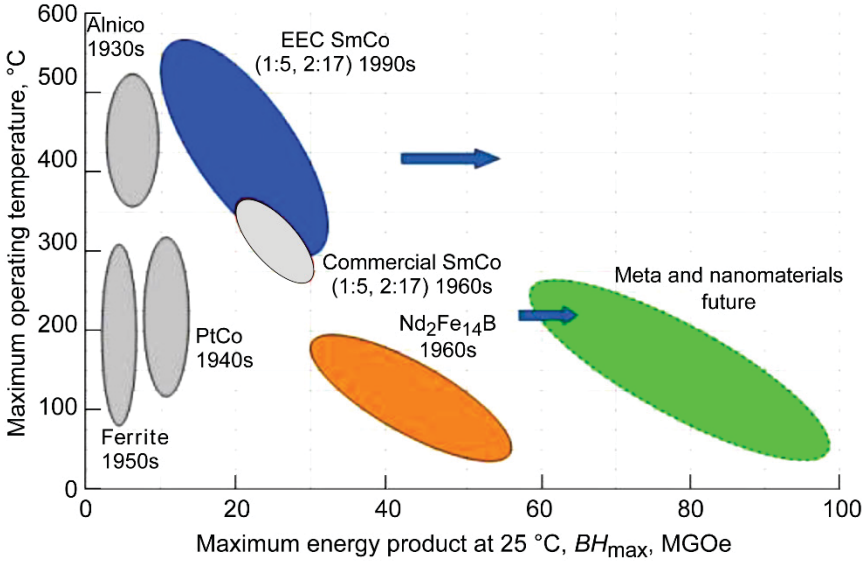

Figure 25.—PM operating temperature versus energy product for existing and future permanent magnets (Ref. 46). Alnico is an alloy primarily consisting of Al, Ni, and Co; SmCo, samarium cobalt magnet; PtCo, platinum cobalt magnet; $Nd_2Fe_{14}B$, neodymium iron boride magnet. Copyright Electron Energy Corporation (EEC); used with permission.

TABLE 5.—PERMANENT MAGNET BENEFITS SUMMARY

Magnet characteristics	State of the art	+15 years	+30 years
NdFeB permanent magnet (PM) remanence, B_r, T	1.51	1.58	1.65
Nanocomposite PM remanence, B_r, T	Unknown	1.75	2.0
NdFeB-only motor (increase in hp/lb), percent	----------	4.6	9.3
Nanoscale PM considered (increase in hp/lb), percent	----------	16	32.4

2.3.3 System Benefits of Motor System Power-Density Improvements

For a one-dimensional model of a Halbach-type motor, torque is directly proportional to the air-gap field, and horsepower is directly proportional to torque. Assuming that the motor design is such that the negative slope of the circuit load line keeps it above the knee of the demagnetization curve, air-gap flux is proportional to B_r. Predicted future benefits of higher B_r are listed in Section 2.3.4.

2.3.4 Summary of Benefits of Permanent Magnets

Table 5 summarizes the estimated magnet properties and resulting system benefits expected in 15 and 30 years.

2.4 Thermal Management

Thermal management provides benefits to motors in terms of both efficiency and specific power. For example, if a motor is cooled, the copper conductor will have lower resistance, which lowers the I^2R heat loss and improves efficiency. Cooling provides benefits to other materials as well. For example, wire insulation has a maximum temperature limit, and PM strength decreases with temperature. With cooling, the motor could be run at a higher power without impacting component temperatures, thereby increasing the specific power of the motor. Thermal management can also improve the efficiency of the associated motor electronics.

Figures 26 and 27 (from a Boeing contractor report for NASA on Subsonic Ultra Green Aircraft Research (SUGAR), (Ref. 3)) show potential configurations for hybrid electric and turboelectric configurations. In both cases, the motor turns the fan rotor shaft. The heat produced by the motor will need to be moved to a heat sink, which could be the bypass air stream, the airframe, the aircraft fuel, batteries, or even a phase-change material that stores the heat temporarily. For the turboelectric configuration (Fig. 27), a likely heat sink is the bypass air, which might even confer an efficiency benefit as a low-grade afterburner.

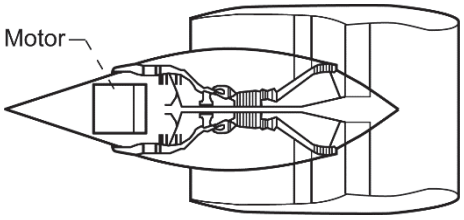

Figure 26.—SUGAR Volt hybrid electric concept (Ref. 3).

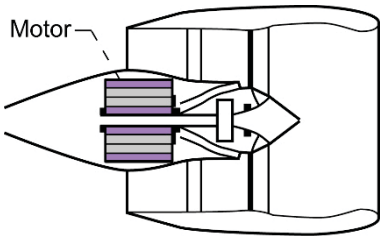

Figure 27.—SUGAR Volt turboelectric concept (Ref. 3).

2.4.1 State of the Art of Thermal Management

Lightweight thermal management could be accomplished by (1) cooling within the motor itself, (2) transferring heat away from the motor to a heat sink, (3) incorporating cooling into existing structures (multifunctional structures), or (4) using new lightweight, highly conductive materials (Fig. 28). The type of cooling used has a direct impact on the current density allowable in the conductor. The higher the current density is,

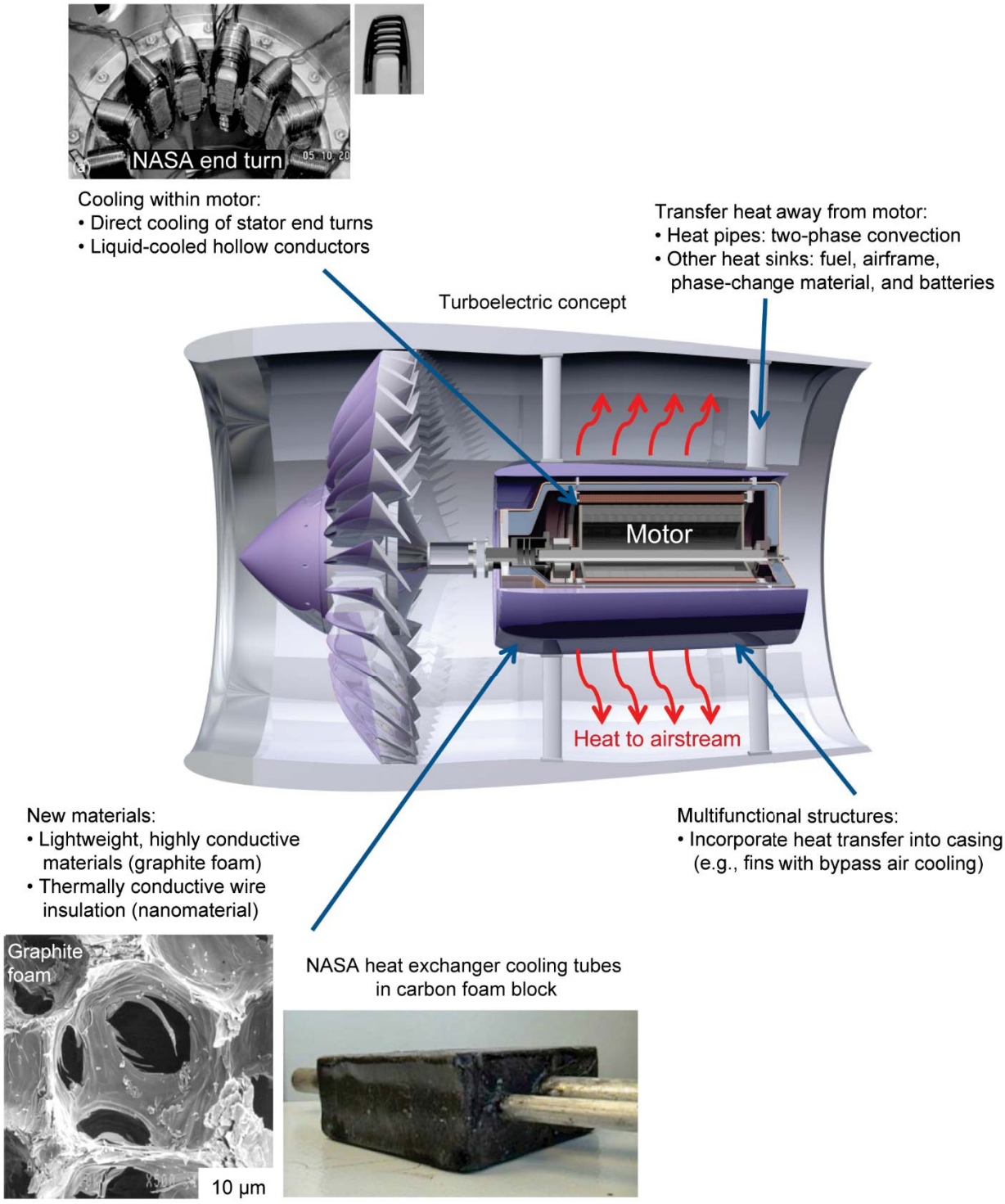

Figure 28.—Advanced thermal management concepts (Refs. 47 to 49). *Graphite foam* photograph reprinted from Carbon, vol. 41, Gallego, Nidia C.; and Klett, James W., Carbon Foams for Thermal Management, pp. 1461–1466. Copyright 2003, with permission from Elsevier.

the tighter the conductor can be packed into the stator slot. This in turn affects the size of the stator, so a higher current density will result in a smaller motor. Figure 29, based on information from Gieras (Ref. 50) shows typical current densities for various cooling techniques.

The I^2R losses from the end turns of motor windings account for a significant portion of the total copper loss. Ways to conduct heat from these end turns include using potting compounds with heat conductive particles, direct stator end turn cooling, or hollow conductors.

Conduction through the structure could provide a path for the heat to travel to the heat sink. Both single-phase and two-phase convection are also available, with two-phase convection (e.g., evaporative cooling) giving the highest heat transfer rate. An active system will yield higher cooling than a passive system, but it will also add weight. Lawson and Pointon (Ref. 51), Lowe (Ref. 52), and Ohadi (Ref. 53) discuss many different means of providing heat transfer from motors used for electromechanical actuators in aircraft and/or harsh environments. Ultimately, the optimal type will depend on the motor size, location, configuration, and required heat transfer rate.

For the aircraft application, Filburn, Kloter, and Cloud (Ref. 54) state that compact heat exchangers are often used in aircraft engines, specifically for cooling engine fluids. They are typically heavy, for example, over 23 kg (50 lb) for a 35-kW (2000-Btu/min) heat exchanger. Filburn et al. showed that simple changes in design and materials can improve the weight significantly, with a concept using bypass air as the heat sink. This type of heat exchanger could fit nicely within the hybrid electric or turboelectric concept.

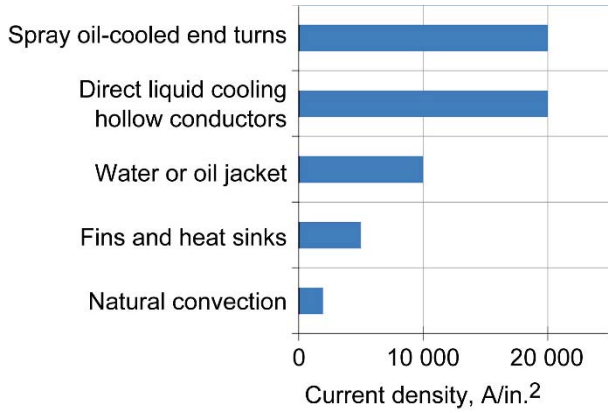

Figure 29.—Current densities for various cooling concepts (Ref. 50).

2.4.2 Possible Improvements to Thermal Management

New materials are expected to improve the thermal management of motors considerably. One of the biggest impacts could be through the use of thermally conductive electrical insulators for the motor conductor. One such material might include nanofibers—such as the polyethylene nanofibers with high thermal conductivity and low electrical conductivity being investigated at the Massachusetts Institute of Technology (Refs. 55 and 56). Table 6 shows the thermal conductivity of individual chains of these nanofibers. Another material is the electrical insulator with BNNTs discussed in Sections 2.2.2 and 2.2.3.

We expect that, in the future, carbon-fiber-composite materials will compose significantly more of the aircraft structure, reducing the total weight. Conduction is expected to be lower because of the reduced thermal conductivity of carbon-fiber-composite materials in comparison to metals (Ref. 51). However, research is being done to develop new thermally conductive composite materials. Oak Ridge National Lab has come up with high-thermal-conductivity graphite foams that have a specific thermal conductivity that is significantly higher than that of copper or aluminum (Ref. 47 and Fig. 28). This kind of material, which was used at Glenn to develop a lightweight heat-exchanger prototype for space applications (Ref. 48 and Fig. 28), could be used in conjunction with a convective heat-transfer system to provide thermal management with lower weight than today's systems. Table 6 shows some values for the thermal conductivity of various materials as given in References 56 and 57. Clearly copper has the highest thermal conductivity of all the materials shown. However, its specific thermal conductivity is well below aluminum, graphite/epoxy composite, and carbon foam.

TABLE 6.—THERMAL CONDUCTIVITY OF CANDIDATE MATERIALS

Material	Density, g/cm^3	Thermal conductivity (in-plane), W/m-K	Specific thermal conductivity (in-plane), W/m-K/(g/cm^3)
Copper (Ref. 57)	8.9	398	44.7
Aluminum (Ref. 57)	2.7	247	91.5
E-Glass/epoxy composite (Ref. 57)	2.1	0.16 to 0.26	0.1 to 0.2
Discontinuous carbon/polymer composite (Ref. 57)	1.7	10 to 100	6 to 59
Natural graphite/epoxy composite (Ref. 57)	1.94	370	190
Carbon foam (Ref. 57)	0.6 to 0.9	135 to 245	220 to 270
Low-electrical-conductivity polyethylene nanofiber (Ref. 56)	----------	104	----------

Cooling could be incorporated into the motor structure itself, as is currently done with liquid-cooled casings. Glenn researchers developed a new coil design for cryogenic switched-reluctance motors, which could also be cooled noncryogenically. These "self-finned coils" were designed to improve heat transfer from the end turns by allowing the cooling fluid to pass through the end turns, making higher current possible (Ref. 49 and Fig. 28). This design could be combined with high-thermal-conductivity nanofiber insulation. Another self-cooling concept is one incorporated within LaunchPoint's Halbach motor, which is air cooled by a fan integrated into the rotor itself (Ref. 10).

The thermal management solution should be optimally incorporated within the aircraft structure design itself. A thoughtful solution will include thermal paths in addition to the other critical parameters, including strength, weight, and aerodynamics. For example, by using new thermally conductive composite materials in conjunction with the bypass air as the heat sink, the finned surface heat exchanger in Reference 54, used to cool engine fluids, achieved a weight reduction of 73 percent versus the baseline heat exchanger. An additional weight savings was expected through incorporating the heat exchanger within the engine case directly adjacent to the bypass stream. This unit was designed to have a heat transfer rate of 35 kW (2000 Btu/min). The baseline unit mass was approximately 23 kg (50 lb), and the lightweight designs were 11.5 kg (25.4 lb) for an aluminum unit and 6.1 kg (13.5 lb) for a carbon-carbon unit. All of this was accomplished through thoughtful design, using technology and materials available today. Benefits will increase with the advanced materials being developed for future use.

2.4.3 System Benefits of Thermal Management Improvements

To get a sense of the amount of heat loss expected in the current study, we plotted the heat produced by the motors per megawatt of power (Fig. 30) for 95- to 98-percent motor efficiency. Each percent increase in efficiency over 95 percent decreased the heat loss by about 5 kW. Clearly, motor design and material improvements (e.g., conductor material and magnet material) that increase efficiency can significantly improve the thermal management problem.

Decreasing the winding temperature will improve the motor efficiency. The efficiency of a Halbach motor depends on the resistance of the motor windings. Merritt et al. (Ref. 58) show that the equation for the efficiency is $\eta = R_L/(R_O + R_L)$, where R_L is the load resistance and R_O is the winding resistance. Reducing the winding resistance has a clear impact on the efficiency. The temperature coefficient α for the resistance of copper is $3.9\times10^{-3}\ °C^{-1}$, meaning that each degree centigrade of increase in temperature over room temperature results in a 0.39-percent increase in resistance and therefore, loss of efficiency. The efficiency equation shows that for an R_O/R_L ratio of approximately 0.04, a 70 °C decrease in copper conductor temperature can increase efficiency from 95 to 96 percent, reducing heat loss by about 5 kW for the 1-MW motor.

Note that the maximum heat shown of 26.3 kW for 95-percent efficiency is comparable to that of the heat exchanger in Reference 54 (35 kW). Assuming a specific power of 4.9 kW/kg (3 hp/lb) and 95-percent efficiency, the mass of the 1-MW motor using today's technology would be around 215 kg (470 lb), and the carbon-carbon heat exchanger unit from Reference 54, sized for a 26.3-kW heat load, would add less than 3 percent to the mass.

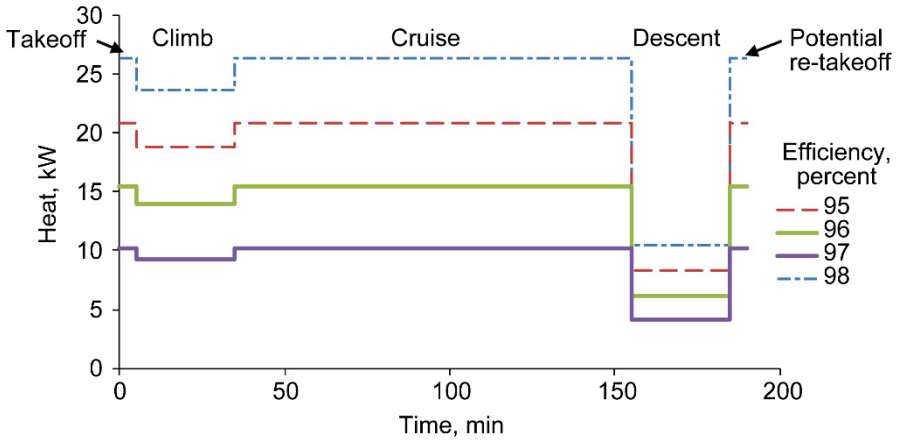

Figure 30.—Heat produced during flight for a 1-MW motor.

Benefits based on making material changes to this heat exchanger were predicted for 15 and 30 years into the future. In 15 years, we expect to use a carbon-fiber-composite material with relatively high thermal conductivity and lower density. The 15-year estimate is based on a carbon-fiber-composite material with a motor efficiency of 95 percent for same-temperature operation. Within 30 years, new nanomaterials will be available with even higher thermal conductivity, leading to lower temperature motors with lighter heat exchangers. The 30-year estimate is based on materials with high specific thermal conductivity and a motor efficiency of 97 percent for lower temperature operation.

To see how the thermal management system could affect the motor power density, a simple analysis was done to predict how increased current density could decrease motor size for the same power level. Assuming that the state-of-the-art stator conductor slot would be 25 percent of the motor cross-sectional area and that the back-iron thickness and rotor size would stay the same, doubling the current density would reduce the motor cross-sectional area (and therefore mass) by 22 percent, increasing the motor power density by 28 percent. If the current density quadrupled, the motor cross-sectional area would decrease by 33 percent, increasing the power density by 49 percent.

2.4.4 Benefits Summary of Thermal Management Improvements

Table 7 summarizes the expected benefits in heat exchanger mass and power density due to thermal management improvements.

2.4.5 Path Forward for Thermal Management

To realize the potential improvements described here, research must be conducted in several areas. First, new materials with high thermal conductivity must be developed. These include materials for the heat exchanger as well as for wire insulation within the motor itself. Oak Ridge National Laboratory has already developed a graphite foam with very high specific conductivity, and the addition of nanofibers could increase conductivity even further. Nanomaterials are also being investigated for high-thermal-conductivity materials that also have low electrical conductivity. These materials could be used as part of or around the winding insulation, providing the greatest impact on heat transfer.

As motor concepts and materials are developed, a thermal analysis must be performed for each configuration to determine the heat transfer requirements. This analysis should include any new materials (wire, insulation, magnets, and/or thermal conductors) in addition to any heat exchanger concept. Testing will be required to evaluate the effectiveness of these new materials and concepts.

As the hybrid electric or turboelectric application becomes better defined, a systems study should be performed that encompasses all aspects of thermal management, including the weight benefit and the efficiency benefit of operating at a lower temperature.

2.5 Structural Weight Reduction

Motor structures include the rotor, stator, back iron, and related components, such as the motor frame, brackets, supports, rotor containment, and housing. For future electric aircraft, the motor structures need specific strength improvements to allow for higher loads at lighter weight when the rotor is operating at high speed, resulting in power density improvement. Thus, a new material development incorporating CNTs is discussed in Sections 2.5.1 to 2.5.4 to identify potential improvements in material properties—such as tensile strength, high-cycle fatigue, and stress rupture. In particular, a high-speed rotor and/or a rotor retention ring that contains and positions the high-speed rotating magnets would be crucial technology developments. Trends in improving composite filament strength are presented, and reasonable estimates of further improvement in 15 and 30 years are projected.

Table 8 shows the approximate distribution of motor structures to the total motor weight for the 60-kW interior PM motor for the 2010 Prius automobile (Ref. 8). The dominant weight components of motors are the stator core, rotor core, and casing. The weight of these components could be reduced dramatically if advanced material and fabrication processes are developed, the use of polymer composites and composites reinforced with nanofibers is increased, and multifunctional structures with thermal management capability are utilized. In addition, the thickness of the electrical insulation of the copper windings could be decreased if advanced materials are used.

TABLE 7.—PREDICTED BENEFITS FROM IMPROVEMENTS IN MATERIAL SPECIFIC CONDUCTIVITY

Improvement	State of the art	+15 years	+30 years
Reduction in heat exchanger mass/MW, kg	17	4.6	1.5
Increase in current density, percent	---	200	400
Decrease in motor weight, percent	---	22	33
Increase in motor power density (hp/lb), percent	---	28	49

2.5.1 State of the Art of Lower Weight Structures

Polymer matrix composites have a very high specific strength (~1000 kN-m/kg for carbon fiber composites compared with ~100 kN-m/kg for stainless steel). This makes them ideal candidates for use in aircraft, where reducing weight is critical. As shown in Table 9, candidate fibers for composite structures include glass fibers, aramid fibers, and carbon fibers. Currently, carbon fiber has the highest tensile strength.

CNTs are the strongest and stiffest materials yet discovered. This strength results from the covalent bonds formed between the individual carbon atoms. As stated in Section 2.1.1, in 2000, tests showed that a multiwalled CNT had a tensile strength of 63 GPa (Ref. 59). Further studies, conducted in 2008, revealed that individual CNT shells have strengths of up to ~100 GPa (Ref. 60). Because of the extraordinary mechanical properties of CNTs—high Young's modulus, high tensile strength, and high thermal conductivity, researchers are studying the use of CNTs to improve the strength of composite materials. We are proposing that CNTs be incorporated into currently existing materials to improve the material properties of high-speed motor structures.

TABLE 8.—MOTOR COMPONENT MASSES FOR 2010 PRIUS MOTOR
[From Ref. 8.]

Component	Mass, kg
Motor	22.7
Stator	16.0
Casing	14.1
Rotor	6.7
Copper	4.9
Permanent magnets	.8
Total mass (motor and casing)	36.8

The literature survey shows that incorporating small volume fractions of multiwalled CNTs in a matrix significantly increases the tensile strength, high-cycle fatigue strength, and durability. Thus, this work aims to investigate and predict the optimal material improvement from utilizing CNTs, on the basis of assumed CNT material properties in 15 and 30 years. Currently, no commercially available materials are reinforced with CNTs.

2.5.2 Possible Improvements From Adding Carbon Nanotubes to Materials

Carbon fiber composites provide the baseline for the candidate material strength. Improvements in strength through the addition of CNTs were projected using assumed fiber strengths of 50 GPa in 15 years and 200 GPa in 30 years. Adding today's CNTs to existing composite materials could nearly double their tensile and fatigue strengths (Refs. 61 and 62).

For calculating the projected values, we assumed that composite strength is a function of fiber strength. The nanofiber composites were assumed to have the same ratio of composite to fiber strength as for Toray T1000 (carbon fiber). For example, T1000 composite has a tensile strength of 3.04 GPa, and the fiber has a tensile strength of 6.37 GPa. Therefore, the composite strength to fiber strength is (3.04/6.37)100 percent = 47.7 percent. We expect that stress rupture and fatigue will reduce the tensile strength and that the derated value will depend on how the material is used—total length of time (stress rupture) and number of cycles (fatigue). In this study, a derating of 50 percent was assumed for the composite materials, and the specific tensile stress (stress/density) was calculated accordingly. Table 9 shows the resulting tensile strengths for proposed composites with nanofibers in comparison to existing materials.

TABLE 9.—TENSILE STRENGTHS OF CURRENT MATERIALS

Material	Tensile strength, GPa	Derated tensile strength, GPa	Typical density, kg/m^3	Specific tensile strength, kN-m/kg
Composite with 200-GPa nanofiber (predicted)	95.4	47.7	1570	30 400
Composite with 100-GPa nanofiber (predicted)	47.7	23.9	1570	15 200
Composite with 50-GPa nanofiber (predicted)	23.9	11.9	1570	7 600
Carbon fiber composite with nanotubes (predicted)	6.08	3.04	1570	1 940
Carbon fiber composite	3.04	1.52	1570	970
Aramid composite	1.10	.55	1400	390
E-Glass composite with nanotubes	2.40	1.20	2000	600
E-Glass composite	1.20	.60	2000	300
Titanium alloy	.95	.95	4430	210
Stainless steel	1.0	1.0	7800	130
Aluminum alloy	.31	.31	2700	110

For advanced motor development, new high-strength materials also could be used to improve primary and secondary motor structures, such as the high-speed rotor and shaft, rotor containment sleeve, motor core support, and electric cable core. For example, for a PM retention ring (Fig. 31), the ring hoop stress is proportional to the square of the motor rotor speed; thus, a higher strength retention ring would allow the rotor to spin faster, leading to high power density. In other words, we could increase power by increasing the material strength. For flywheel energy storage, carbon nanofiber rotors, which can have very high strength-to-weight ratios, would give flywheels the potential for high specific energy.

Another approach to reducing motor weight is the development of advanced manufacturing techniques. For example, using screen printing to manufacture windings for motors could reduce motor weight. One company uses an etched copper sheet to fabricate the coil, allowing for a higher packing ratio (Ref. 64).

2.5.3 System Benefits of Low-Weight Carbon Nanotube Materials

Table 10 quantifies and summarizes, for 15 and 30 years into the future, the projected advancements of material characteristics based on anticipated CNT tensile stress estimates, carbon nanofiber stress improvements, and the advanced manufacturing techniques mentioned in Section 2.5.2. The predictions assume the use of high-strength, lightweight materials throughout the motor and supporting structures, with benefits similar to those for aircraft structures that use nanotube- or nanofiber-reinforced composites.

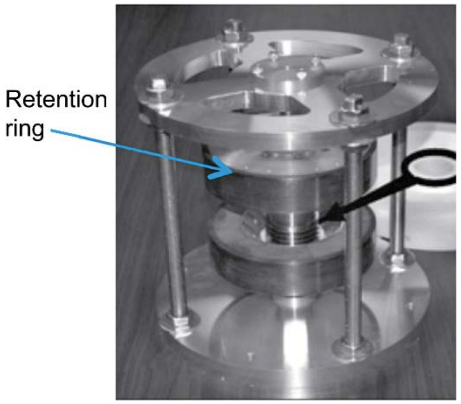

Figure 31.—Ironless Halbach permanent magnet motor (Ref. 63).

2.5.4 Path Forward for Carbon Nanotube Materials

Numerous efforts in developing nanofibers are ongoing, but the fabrication process is very limited and in its infancy. Glenn has begun investigating composite materials for high strength and low cost, but additional work needs to be done to mature carbon-fiber and CNT material technologies. Small batches of fiber need to be produced with consistent properties. Strength, fatigue, creep, and environmental effects need to be characterized. In addition, the best material system needs to be brought up to production levels. This work needs to be continued for several decades to achieve stronger and stronger composite materials. This would ensure that, 30 years from now, commercial products utilizing nanofibers are available for motor structures.

2.6 Bearingless Motor Technology

One possible configuration to improve the power density and system reliability of motors is to employ a bearingless motor, which can eliminate conventional mechanical bearings and the associated complex bearing lubrication system. This would significantly increase power density and extend life.

The bearingless motor concept stems from active magnetic bearing technology, which uses the principle of electromagnetic suspension. As shown in Figure 32 (Ref. 65), it consists of an electromagnetic assembly, a set of power amplifiers that supply current to the electromagnets, a controller, and gap sensors with associated power electronics to provide the feedback required to control the position of the rotor within the gap. Numerous efforts have been made to develop a variety of magnetic bearings for turbomachinery applications, accomplishing tangible technical milestones. However, the practical application of magnetic bearings to turbomachinery may be limited because of the additional subsystem weights necessary to improve system reliability, redundancy, and performance.

TABLE 10.—STRUCTURAL MATERIALS BENEFITS SUMMARY

Improvement	State of the art	+15 years	+30 years
Structural weight reduction, percent	---	25	50
Power density, hp/lb	3	4	6

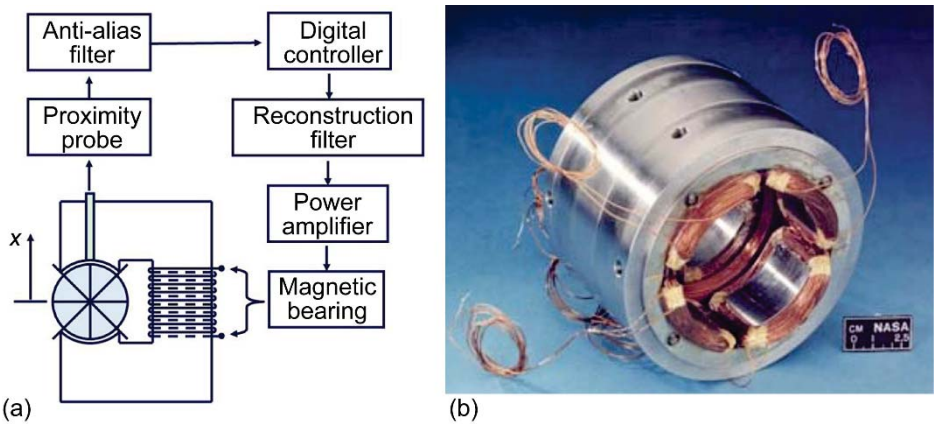

Figure 32.—Active magnetic bearing components. (a) Schematic of magnetic bearing and control system (Ref. 65). (b) Active magnetic bearing stator.

However, the motor drive power electronics and control systems that are associated with electric motors are key components to the implementation of a magnetically suspended rotor system. An electric bearingless motor (also called an "integrated motor-bearing" or "self-bearing motor") combines the magnetic bearing and motoring functions into magnetic actuators that produce both radial force and torque. Such a design can eliminate conventional mechanical bearings and their complex lubrication systems, resulting in weight reduction, maintenance cost savings, extended life, and improved reliability. Furthermore, vibration isolation of the electric motor drive is possible through proper feedback control of the radial (or magnetic bearing) force generation (Ref. 66).

Thus, the bearingless motor is a strong candidate for a high-power-density motor for future electric propulsion systems. In the sections that follow, the bearingless motor was investigated to identify and characterize variables that could improve power density, system reliability, and redundancy for fail-safe operation. Also, reasonable power-density improvements resulting from the bearingless motor technology were evaluated and projected for 15 and 30 years into the future.

2.6.1 State of the Art of Bearingless Motors

The bearingless configuration superimposes the magnetic bearing function and motoring function by adding a separate magnetic bearing coil winding to each stator pole motor winding for rotor levitation (two coils per stator pole). This feature looks like a bearingless motor, but it requires additional magnetic bearing coils and an electrical subsystem for the extra coil windings. During the last decade, this approach has been used by many researchers for a variety of motors, including PM (Ref. 67), induction (Ref. 68), synchronizing-reluctance (Ref. 69), and switched-reluctance types (Ref. 70).

Figure 33.—Eurocopter equipped with bearingless rotor hub (Ref. 71). © Eurocopter, now Airbus Helicopters; used with permission.

Unfortunately, a bearingless configuration also decreases the power density by adding the levitation coil windings and associated extra power electronics into the existing motor configuration. Furthermore, it produces coupled magnetic flux on each stator pole, resulting in inefficient control efforts.

State-of-the-art bearingless motors have been demonstrated in research laboratories, and in recent progress on rotorcraft, a bearingless rotor hub was demonstrated by Eurocopter (Fig. 33). Key characteristics of the new bearingless rotor (Ref. 71) are its extremely compact and lightweight rotor hub and its improved flight characteristics.

2.6.2 Possible Improvements to Bearingless Motors

Here we propose a novel bearingless motor system, where only one coil winding per stator pole can perform both radial force (magnetic bearing) and torque production (motoring). This feature would play an essential role in developing a high-power-density motor because it can eliminate additional

levitation coil windings and the associated power electronics, resulting in an authentic bearingless motor. We selected a switched-reluctance motor (SRM) to explain the working principle of this bearingless motor system because the SRM's inherent fault tolerance, robustness under high temperatures, and rotor reliability at high rotational speeds (no coil windings on the rotor) make it a potential candidate for future airborne systems. However, compared with standard rotor-type motors, this SRM has a salient rotor structure, so it requires a highly nonlinear dynamics characterization process and analysis. Because of this system complexity, the SRM has historically been omitted for consideration as a candidate motor type for future electric propulsion.

As shown in Figure 34, only one coil winding is wound per stator pole. For room temperature operation, the coil currents must be minimized so that core flux production is limited to the linear region of the core material *BH* curve to avoid magnetic saturation. The required motoring and levitating currents are summed and go into a single motor coil per pole. This enables the highest power output of the motor because it allows more space for motor coil windings (high-power-density feature).

From a controls perspective, a practical observation-based controller using a proportional-derivative control algorithm can be developed to avoid mathematical complexity, thereby providing faster real-time calculation and allowing a much higher rotor speed. This simpler algorithm could significantly reduce controller development time and cost.

Further power-density improvements could be achieved with CNT conductors, which can produce higher current density and significantly reduce weight. However, such conductors were out of scope for this section, and only copper windings were considered for the bearingless motor study. Further advances in the material characteristics of copper were assumed to be negligible 15 and 30 years in the future.

2.6.3 System Benefits of Bearingless Motors

This novel bearingless configuration would significantly contribute to developing a higher power-density motor. It also would extend life, eliminate the contact of moving parts, extend the operating temperature range, and improve rotordynamic control. The following list summarizes the innovative features and associated benefits in terms of hardware and software:

(1) Significant system-level weight reduction would be achieved by eliminating mechanical bearings and the associated lubrication system. According to an estimate of the weight for a cryogenic electric system for the turboelectric propulsion system that is being modeled for a Boeing 777 class aircraft, the weight savings for the propulsor would be on the order of 5.3 percent and the weight savings for the generator would be on the order of 5.4 percent. However, the weight savings for the noncryogenic copper windings for a Boeing 737–400 class aircraft would be much higher because of the large bearing size and lubrication system. Thus, a 10-percent weight reduction is the best estimate (in the case of copper windings).

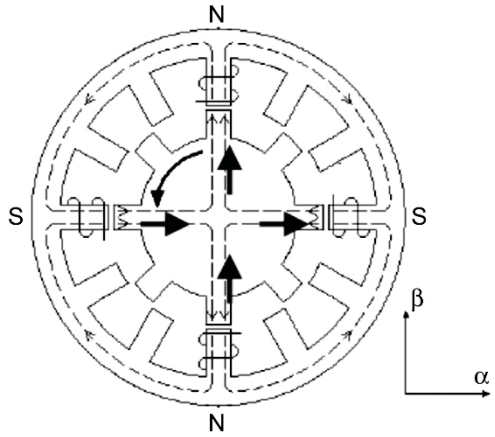

Figure 34.—Phase A motor winding configuration and levitation currents polarity of the 12–8 SRM (Ref. 72).

(2) Additional motor-level weight reduction could be achieved by eliminating separate levitation coils and the associated power electronics. An additional 10-percent weight savings would be a reasonable estimate.

(3) System reliability would be improved. The inherent fault tolerance and redundancy feature would enable continuous operation even after partial failures of the electronics or coil wirings.

(4) Maintenance costs would be reduced. Cost benefits include improving motor efficiency by 0.5 to 1.0 percent, eliminating oil consumption, reducing costs for rotor support system maintenance, and reducing acquisition costs.

(5) Design time and costs for developing the bearingless motor and controller would be reduced significantly. The implementation process does not require a new motor design but uses motor winding coils in a conventional motor configuration. Also, the adaptive controller, which uses a gain schedule scheme, does not require a complicated mathematical plant model. Thus, it can be implemented in real time at much higher rotor speeds.

(6) However, because only one motoring coil winding is used for each stator pole to produce the levitation force, a fraction of the motoring coil current might be used for the magnetic bearing force. Consequently, 5-percent motoring power loss would be a reasonable estimate.

2.6.4 Summary of Bearingless Motor Improvements

On the basis of the anticipated weight reductions and power loss described in Section 2.6.3, the projected improvements of power density and characteristics for 15 and 30 years into the future were quantified and summarized in Table 11. It was assumed that noncryogenic copper windings would be used, and no hardware modification was done for this study. We concluded that employing the proposed bearingless technology would improve power density by more than 20 percent.

TABLE 11.—PROJECTED VALUES OF COMPONENT AND MOTOR LEVEL IMPROVEMENT.

Improvement	+15 years	+30 years
Motor-level efficiency, percent	1.0	1.5
Increase in motor-level power density (hp/lb), percent	20	22
Maintenance cost savings (Ref. 73), million $/plane/year	~1	~2
Durability increase because of elimination of additional coils and power electronics, percent	80 (durable probes)	90 (no probes)

2.7 Power Electronics

Two types of components are considered in this section: rectifiers and inverters:

(1) In the turboelectric system, power is provided at the generator output as AC. This power must be converted to direct current (DC) and then made available to other systems on the DC bus. Rectifiers are used to convert AC power to DC power.

Rectification can be performed using several approaches. Passive rectification, using semiconductor diodes, is a simple approach: the bridge rectifier is one example. However, the use of diodes is inefficient because of the inherent voltage drop across the diodes.

We considered active rectification, or synchronous rectification, instead. This technique improves the rectification efficiency by replacing the higher loss diodes with actively controlled switches. It also allows active power factor correction and other improvements.

(2) Inverters are used to change the DC from the bus (provided by generator and/or energy storage) to AC for the variable-speed motor drive for propulsion. Inverters enable a difference between the fan speed and the engine's power shaft speed, effectively acting like a gear box with a variable ratio. Figure 35 shows a typical inverter configuration using six switches. The DC voltage is converted to AC in motor phases A, B, and C.

Typically, for both inverters and active rectifiers, filtering is used at the input and the output: a DC bus capacitor on the DC side, and an output filter on the AC side. Both bus caps and output filters can add considerable mass to the power electronics system.

2.7.1 State of the Art of Power Electronics

In this application, the active rectifier and the inverter are similar in structure; they are both composed of packaging, sets of power switches, and input and output filtering. Thus, the state-of-the-art performance of both systems is similar, and improvements would benefit both equally. Therefore, to simplify the discussion, only the present and potential future performance of inverters is discussed, with the understanding that inverter advances will similarly benefit active rectifiers.

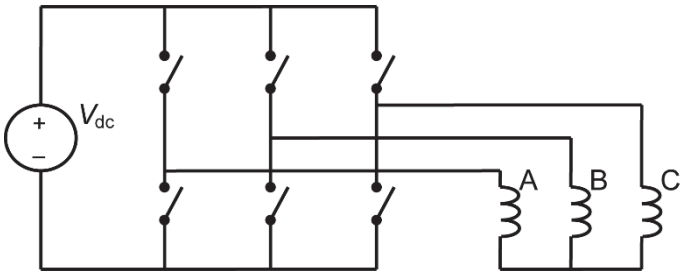

Figure 35.—Inverter schematic. V_{dc}, direct-current voltage.

Power density and efficiency are the key performance metrics for inverters. Although greater performance is available under laboratory conditions, the state-of-the-art power density for inverters is 5 hp/lb (Ref. 74), and state-of-the-art efficiencies are in the 93- to 95-percent range (Ref. 75).

The configuration shown in Figure 35 is a common topology for state-of-the-art inverters, but improved topologies exist. The filtering at the input and output of the inverter, required on the DC and the AC side for many applications, contributes considerable mass and volume, affording another improvement opportunity. In addition, silicon is the semiconductor used in the majority of devices today, but improved materials are being developed. These potential improvements are discussed in Section 2.7.2.

2.7.2 Possible Improvements to Power Electronics

A number of possible approaches are available to improve the power density and efficiency of inverters, including improved switching components, new material types, advanced switching topologies, improved filtering components, improved packaging, and improved thermal management. These possible improvements are discussed in Sections 2.7.2.1 to 2.7.2.6.

2.7.2.1 Improved Switching Components

The two main types of losses in inverters are switching losses and conduction losses. In both cases, the power is lost in the switching devices (typically transistors: metal-oxide-semiconductor field-effect transistors, MOSFETS, or insulated-gate bipolar transistors, IGBTS).

Switching losses occur during a transition, as the switch is being turned on or off. While the switch is off, there is no current flow through the switch; and while the switch is on, ideally, there is no voltage drop across the switch. Because power dropped across the switch is equal to the product of voltage and current, there is little power lost under either of these conditions (the "on" or "off" state). However, during switching, there is a finite time when both the voltage across the switch and the current through the switch are simultaneously nonzero, resulting in a net power loss in the switch. This is called switching loss. Decreasing this overlap time, and thus reducing the power lost during switching, is one improvement opportunity. Also more rapid switching can be achieved via the development of improved components, materials, manufacturing processes, and design approaches.

The ideal switch has zero resistance while it is in the "off" state. However, the semiconductor switching devices used in inverters are not ideal. Their resistance while in the "on" state, for example, is not zero. This nonideal performance leads to conduction losses. Improvements in component materials (the development of materials with lower "on-state" resistance) will certainly decrease these losses as well. Also, paralleling devices to lower overall resistance could reduce conduction losses, although this approach might incur a weight penalty.

2.7.2.2 New Materials

Another approach for improving inverter performance is the development of new materials. One very promising material is silicon carbide (SiC). SiC-based power electronics could enable power systems that are significantly more efficient, lighter, and smaller than systems based on silicon electronics (Ref. 76). Benefits from SiC-based components include higher breakdown voltage, lower "on" resistance, higher thermal conductivity, higher operating temperature, higher reliability, and radiation hardness (Ref. 77).

Some SiC-based devices are available now: for example, Schottky diodes and field-effect transistors. However, performance, reliability, and device cost issues persist because of defects in commercially available SiC semiconductor wafers (Ref. 76). Considerable progress can be expected over the next 15 and 30 years, and many more SiC-based power electronic devices should become available in that timeframe. Reference 78 shows that using SiC in an inverter design enabled a 50-percent reduction in module size and a 70-percent reduction in power loss.

2.7.2.3 Advanced Switching Topologies

The six-switch topology (Fig. 35) is very commonly used in inverters. However, advanced topologies can be used to improve performance. Two such advanced topologies are the multilevel inverter and the "soft-switching" inverter.

To generate the output waveform, multilevel inverters use extra sets of switches and an advanced control algorithm. This approach can be used to improve performance in several ways. One way is to generate a precise voltage waveform, with minimum harmonic distortion. This could also be used to provide active power quality control, eliminating the need for output filtering and, thus, saving weight. In addition, the ability to utilize switches of different power levels within the inverter to generate different portions of the output waveform may provide benefits. However, one potential drawback to the multilevel inverter approach is the need for isolated power supplies for the stages, which would have to be traded for weight savings.

Typical inverters are "hard-switching" types, meaning that during switching, nonzero currents flowing through the device and nonzero voltages across the device exist simultaneously, resulting in power loss. Soft-switching inverters are configured so that switching transitions are made while voltage across, or current through, the device is zero. In addition to lowering switching loss, soft switching lowers switch stress and electromagnetic interference.

2.7.2.4 Improved Filter Components

Filter components are typically used on the input (DC bus caps) and output (AC filter) of the inverter. Because these components can contribute significant weight to the inverter, reducing their size would benefit power density.

Current DC bus capacitors occupy a significant fraction of the volume and weight of inverter modules. In addition, they cannot tolerate high temperatures (>120 °C) and they have poor packaging and inadequate reliability (Ref. 76). Figure 36 shows an example volume breakdown for a 10-kW inverter.

Research is being conducted on dielectric improvements, including polymer and glass materials. Any improvement in capacitor performance could be used to decrease component weight.

Inductors and capacitors are two key components of AC filters. The capacitor improvements discussed in this section could be applied to the AC side as well. Also, any advancement in inductors (magnetic material or conductor improvements) would benefit inductor weights as well, by enabling reduced filter size and weight.

2.7.2.5 Improved Packaging

Improving packaging could improve the performance of power inverters. New packaging concepts could be developed to provide improved electrical performance, reliability, and manufacturability. Other potential benefits include improved ruggedness and, of course, increased power density (Ref. 76).

2.7.2.6 Improved Thermal Management

As devices with higher current-density capability are developed, cooling must also be provided to maintain them at below their maximum allowable temperature. One improved thermal management technique is double-sided cooling, as opposed to single-sided cooling (Ref. 79), allowing multiple

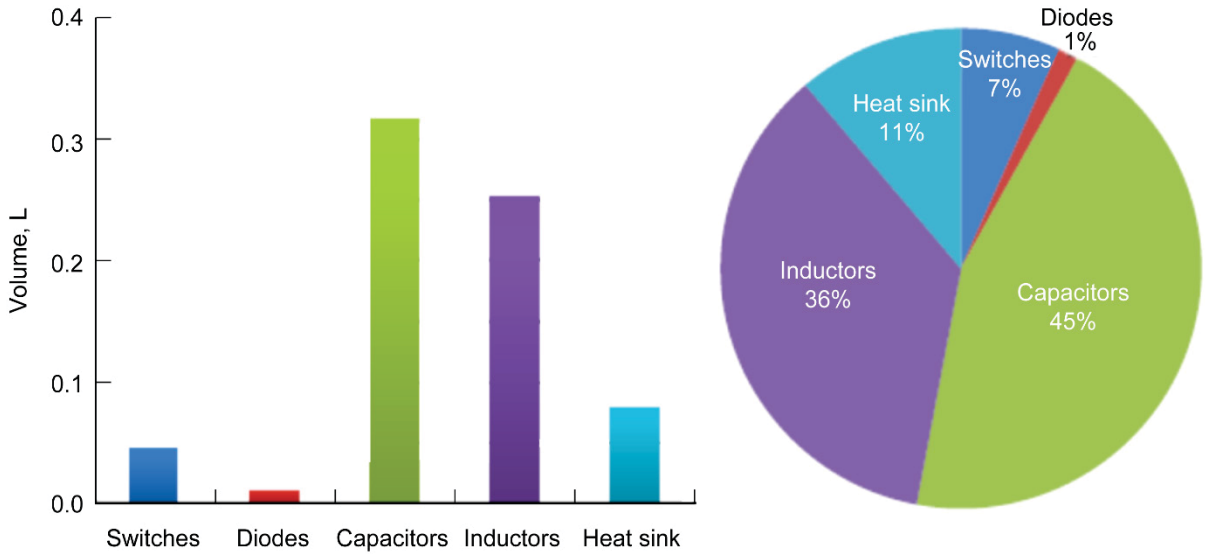

Figure 36.—10-kW Inverter part volume breakdown by liter and percentage (Ref. 76).

TABLE 12.—POWER ELECTRONICS AND SYSTEM IMPROVEMENTS

Power electronics characteristic	State of the art	+15 years	+30 years
Power electronics efficiency, percent	93 to 95	98	99
Power electronics power density, hp/lb	5	10	15
System power density (hp/lb) improvement, percent	0	23	33

cooling paths, thus improving thermal management. Additional advanced cooling techniques are also possible, including direct cooling of the chip itself.

Thermal management is required for other components in the vehicle. Another opportunity is to incorporate power electronics cooling with existing cooling systems. Improved (higher temperature) materials may open up opportunities for part placement to take advantage of this synergy.

2.7.3 System Benefits of Improved Power Electronics

In order to capture benefits, we will consider the system to be the combined inverter and motor. Total system weight for a given power level is then

$$W_s = P_s/D_s \tag{2}$$

where W_s is the system weight, P_s is the system power, and D_s is the system power density. In this case, the system power density is composed of the motor and inverter power densities:

$$D_s = \left(\frac{1}{D_m} + \frac{1}{D_i}\right)^{-1} \tag{3}$$

where D_m is the motor power density and D_i is the inverter power density.

The goal is to drive up inverter power densities with the techniques discussed. The potential system benefits because of improved inverter power density can then be described as

$$\text{Power density percent improvement} = \frac{D_s' - D_s}{D_s} \tag{4}$$

where D_s' is the improved system power density, driven by higher D_i.

Estimates of future power electronics power densities were made on the basis of the potential improvement opportunities discussed in Section 2.7.2. Equation (4) and the assumed motor power density of 3 hp/lb were used to calculate system-level improvements. This information is captured in Table 12.

2.7.4 Summary of Power Electronics Improvements

Table 12 summarizes the performance improvement.

2.7.5 Path Forward for Power Electronics

The recommended path forward is to address any or all of the potential improvement areas:

(1) Improved switching components could be pursued, either by funding the production of new components externally

and/or by performing lab tests at Glenn to quantify the benefits of the improvements in actual power electronics systems.

(2) New material technologies could be pursued in a similar fashion. The development of SiC components is ongoing, and funding further efforts and/or integrating components into power electronics systems, as they become available, would further this technology.

(3) Advanced topologies could be developed through research into multilevel and/or soft-switching inverters for hybrid aircraft use. Building, testing, and evaluation of the performance of these inverters would further this technology.

(4) Improved filter components could be approached by funding external research or by performing internal research. New filter dielectrics could be discovered through materials research. Also new glass and new polymer dielectrics could be studied at Glenn, and improved inductors based on new available materials could be developed at Glenn.

2.8 Path Forward for Cumulative Motor Improvement Benefits

Figures 37 and 38 summarize the projected benefits to the motor power density due to each technology in 15 and 30 years, assuming a current state-of-the-art power density of 3 hp/lb. However, a subsequent effort should be performed to evaluate the cumulative effects of motor component improvements on the specific power and efficiency of a representative motor. This effort would predict improvements while considering that each motor component's benefits may interact with other components. This analysis could be done using motor modeling software. A state-of-the-art baseline motor would be chosen, then the expected improved components would be substituted in the model to determine the new specific power and efficiency levels. In addition, this model could be used in conjunction with a thermal analysis to predict the benefits of thermal management.

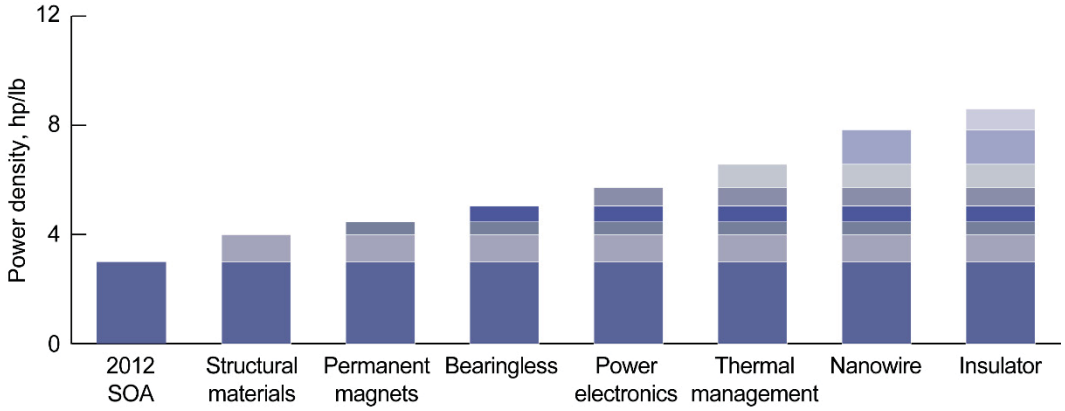

Figure 37.—Projected power density benefits at 15 years for select motor technologies. SOA, state of the art.

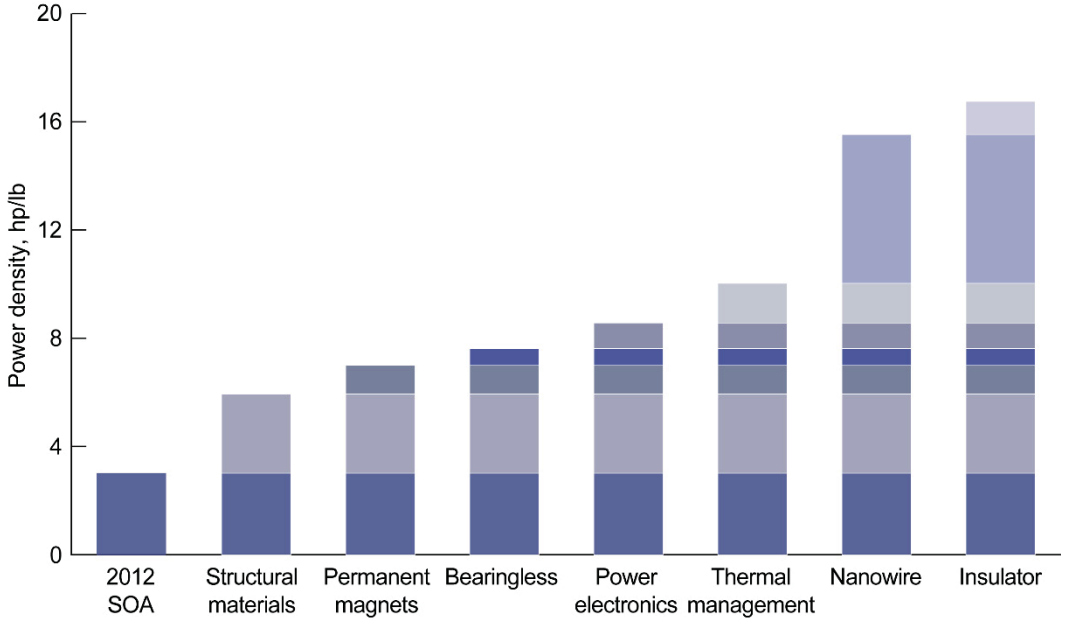

Figure 38.—Projected power density benefits at 30 years for select motor technologies. SOA, state of the art.

3.0 Energy Storage

Hybrid propulsion systems are under consideration for future aircraft, with the power being provided by both an electric energy storage system and a fuel-burning system. Chemical batteries, flywheels, and supercapacitors were considered for energy storage devices. Figure 39, from Kötz (Ref. 80), shows a Ragone plot of the energy density versus the power density of various energy storage devices. Flywheels are not shown on this figure, but they could improve on their energy density in comparison to supercapacitors and on their power density in comparison to batteries. Depending on the demands of the hybrid electric propulsion system, one or more of these devices will be required.

In this study, it was assumed that the propulsive power required during takeoff, climbout, descent, and landing would be shared equally by the electric storage system and the fuel-burning system. The power required during the cruise and taxi phases would be provided solely by the electrical energy storage system.

Two power classes of electric motors were considered in this study: 1 and 10 MW. It was assumed that the motors were 95-percent efficient and that the power inverter was 97-percent efficient. Also, two system bus voltages were assumed: 700 and 1000 V. Table 13 shows the appropriate powers and energies required during each mission segment. The powers listed in Table 13 are average powers for each flight phase; however, the powers required during an actual flight will likely contain many short-term power "spikes" throughout the flight. The energy storage system size must not only provide adequate overall energy and average power but be able to respond to intermittent power spikes. Rather than designing a single-energy storage system (batteries) to accommodate these power spikes, incorporating supercapacitors within the design might enable a smaller overall energy storage system. The supercapacitors would provide power for the spikes and then be recharged via the main energy storage system to provide power for the next intermittent spike. Flywheels, which have a higher discharge rate, may also be employed to handle the power spikes that occur.

The corresponding energy required from the energy storage device for each flight segment and the cumulative energy is shown in Figure 40 for the 1-MW motor and in Figure 41 for the 10-MW motor.

When an energy storage system is sized for this scenario, the cruise portion of the flight has the largest impact. Not only is the motor working at its maximum capability and thus drawing the maximum power from the energy storage system, but the cruise phase is 2 h and makes the largest impact on the overall capacity needed from the system.

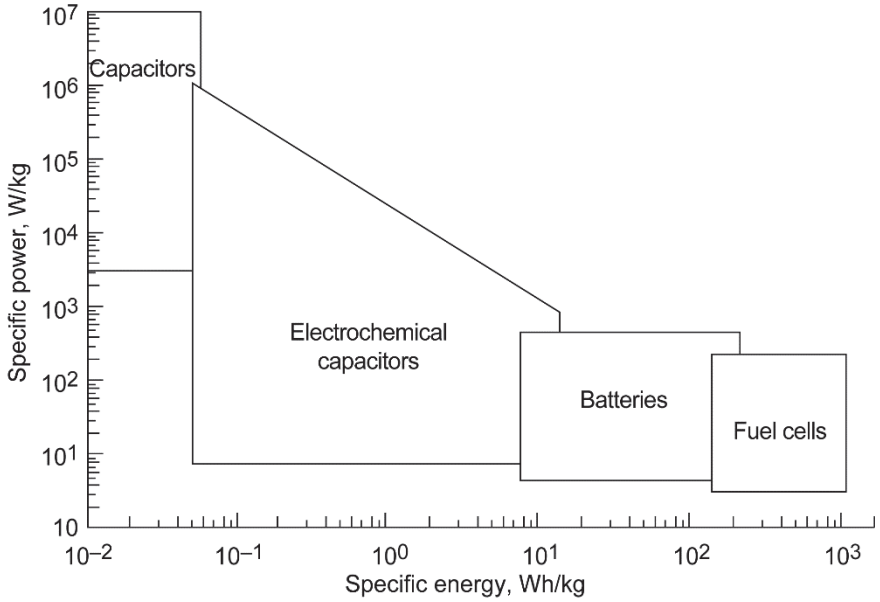

Figure 39.—Ragone plot of energy density versus power density for various energy storage devices (approximate values). Adapted from Reference 80: Electrochimica Acta, vol. 45, no. 15, Kötz, R.; and Carlen, M., Principles and Applications of Electrochemical Capacitors, pp. 2483–2498, Copyright 2000, with permission from Elsevier.

TABLE 13.—ASSUMED MISSION DURATIONS, POWER, CURRENTS, AND ENERGY REQUIREMENTS FOR 1- AND 10-MW ELECTRIC MOTORS

Phase of flight	Duration, min	Power, kW	Current (700 V), A	Current (1000 V), A	Electrical output, kW-h	Cumulative electrical output, kW-h
1-MW-class motor						
Taxi	5	54	77	54	5	5
Takeoff	5	1 082	1 545	1 082	90	95
Climbout	30	973	1 391	973	487	581
Cruise	120	1 082	1 545	1 082	2 163	2 744
Descent	30	216	309	216	108	2 852
Landing	5	1 082	1 545	1 082	90	2 943
Taxi after landing	5	54	77	54	5	2 947
10-MW-class motor						
Taxi	5	541	773	541	45	45
Takeoff	5	10 815	15 450	10 815	901	946
Climbout	30	9 734	13 905	9 734	4 867	5 813
Cruise	120	10 815	15 450	10 815	21 630	27 443
Descent	30	2 163	3 090	2 163	1 082	28 525
Landing	5	10 815	15 450	10 815	901	29 426
Taxi after landing	5	541	773	541	45	29 471

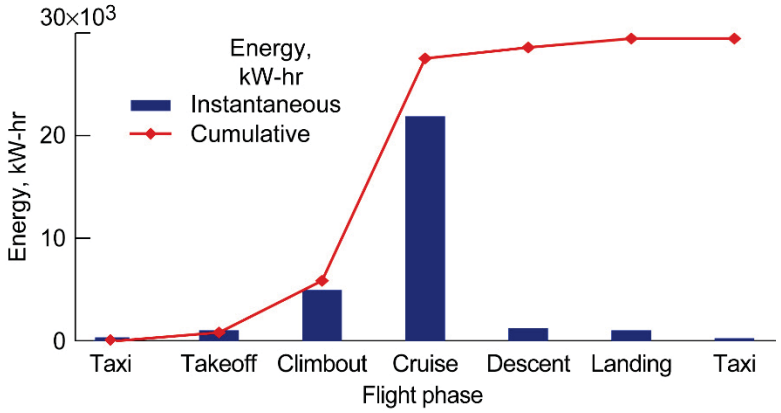

Figure 40.—Energy required for all phases of the flight and the cumulative energy for a 1-MW motor (95-percent-efficient motor and 97-percent-efficient inverter).

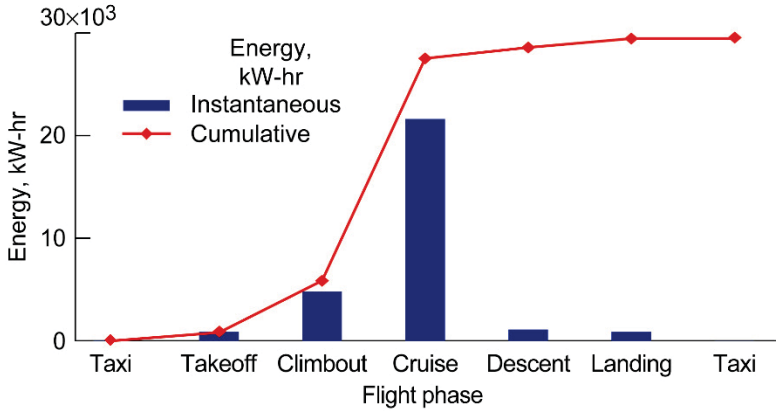

Figure 41.—Energy required for all phases of the flight and the cumulative energy for a 10-MW motor (95-percent-efficient motor and 97-percent-efficient inverter).

3.1 Batteries

In this section, three potential battery chemistries are discussed as candidates for future energy storage for hybrid electric aircraft. A battery is a device that converts chemical energy to electrical energy. Batteries are generally made up of a number of cells. The power, voltage, current, and duration of the application determines how many cells are included in a battery and how they are arranged—for example, the series/parallel arrangement. Battery cells are designed using different chemistries in different sizes, shapes, energy content, voltages, and discharge rates. The specific cell chosen for use in a battery not only depends on the application but on what characteristics are most important: for example, cycle life, weight and volume restrictions, operational temperatures, and charge/discharge time. The complete battery contains the cells or modules, battery management system, thermal management interface, and power takeoffs.

In the quest for higher specific-energy batteries, a number of avenues can be approached. Lighter materials, both active and inactive to the reaction in the battery, can help lower the overall weight of the battery. Although the type and quantity of the anode and cathode material within a cell determine the amount of energy stored within a cell, a mass breakdown of the components within a typical lithium-ion battery shows that the anode and cathode within the cell only make up 57 percent of the overall cell mass (Ref. 81). The remaining cell mass is made up of the electrolyte, current collectors, separators, wiring, and case.

Other methods to improve specific energy include increasing the number of electrons moving through the circuit. This can be done in a number of ways:

(1) Increase the charge carried by the moving ion. However, an ion capable of carrying a higher charge is generally heavier.

(2) Increase the amount of active material within the cell. This not only adds additional mass to the cell but can make it a challenge to fully utilize all the material in the cell.

(3) Lower the resistive losses within a cell via improved conductivity of the battery electrode material, improved current collection design, and improved electrolytes.

(4) Increase the voltage between the cathode and anode, given the same number of electrons passing during the reaction, resulting in a higher power. This approach not only requires electrode materials with higher voltages but an electrolyte that is stable over time at those voltages.

(5) Reduce the weight of battery and cell case structures, current collectors, and wiring without sacrificing performance.

(6) Increase the surface area at the electrode/electrolyte interface to increase the discharge/charge rates and the utilization of the battery material.

3.1.1 State of the Art of Batteries

Currently, the most promising batteries for electric aircraft are based on lithium, which is the lightest metal and will likely lead to the highest specific energy (energy stored per unit mass). Lithium-ion, lithium-sulfur, and lithium-air/oxygen batteries are the most likely candidates. Currently available specific energies, at the cell level, are 80 to 200 Wh/kg (depending on chemistry) for lithium-ion batteries, 250 to 300 Wh/kg for lithium-sulfur batteries, and 300 to 350 Wh/kg for lithium-air/oxygen batteries (Refs. 82 to 84). Lithium-ion batteries are the most mature technology of the three candidates. Although lithium-sulfur and lithium-air/oxygen batteries currently have higher specific energies, they face significant barriers to commercial use, including very limited cycle life.

Figure 42 shows an example of a state-of-the-art lithium-ion battery—the battery used on the Mars Surveyor Lander. It consists of two 25-Ah batteries and has a voltage operating range of 24 to 32.8 V.

In a lithium-ion battery, the lithium shuttles between the anode and cathode electrodes. The materials making up the electrodes are typically layered compounds that allow lithium ions to be inserted between the layers. Improvements in both the cathode and anode could yield significant improvements to the specific energy of a cell. Several options for cathode materials have been included in cells, each with their own pros and cons. However, the cathode is generally made up of transition metal oxides with a layered structure, and these materials have a relatively low capacity for lithium-ion insertion. Recent improvements in the material structure and composition (including dopants) have increased electrode voltage and capacity for lithium ions, but significant work remains (Ref. 81).

Figure 42.—Mars Surveyor Lander battery (two 25-Ah batteries).

Lithium-sulfur batteries have generated a lot of interest for potential inclusion in electric vehicles because of the low-cost materials involved in the construction of the cells and, most importantly, the high theoretical specific energy—greater than 2000 Wh/kg. Current lithium-sulfur batteries contain a lithium metal anode and a sulfur cathode, the sulfur being contained in a carbon electrode matrix. Initial cells produced with this chemistry have been promising, with specific energies of approximately 300 Wh/kg on the cell level (Ref. 85). However, these cells tolerate only a few charge/discharge cycles before significant capacity loss occurs. Several issues are thought to contribute to the loss of capacity over time with cycling (Ref. 86): (1) dissolution of a lithium polysulfide reaction product into the electrolyte, which results in a loss of lithium and sulfur from the anodes and cathodes; (2) morphology changes to the lithium itself, including the formation of dendrites and voids, which lead to short circuits and loss of electrical contact; and (3) dimensional changes in the cathode and anode upon cycling, leading to loss of electrical contact with the active material. Work is ongoing to address these and other problems with rechargeable lithium-sulfur batteries (Refs. 87 and 88).

Lithium-air batteries also are a promising technology, with theoretical specific energies in excess of 3000 Wh/kg (Ref. 89). However, the technology still has a number of technical hurdles to be overcome before it is ready for commercial use. The highest specific energy reported so far has been 344 Wh/kg for a battery-level assembly (Ref. 90), but this was based on a lab-scale cell. Currently, the capacity of lithium-air cells cannot be maintained over multiple charge/discharge cycles; they rapidly lose capacity after only 50 cycles. Several areas will need to be addressed in order to make rechargeable lithium-air/oxygen batteries a reality. The air cathode design needs to be optimized to facilitate the flow of air to the electrode surface. Also, the cathode must effectively handle the lithium-oxygen product. Currently this reaction product blocks the pores of the cathode at the reaction sites and prematurely stops the reaction, limiting battery capacity (Ref. 91). Lithium-metal anodes are prone to dendrite formation upon cycling, which in turn leads to short-circuiting. In addition, resistive barriers are formed on the lithium surface from reaction with the electrolytes and impurities within (Refs. 92 and 93). Stable electrolytes are necessary to facilitate the overall reaction while also limiting or controlling dendrite formation or morphology changes.

From a system-level perspective, substantial work remains in the design of a working battery. Not only must the standard battery construction restraints be included in the design, but provisions must be made to provide adequate air or oxygen to the overall battery, and all the cells within, to maintain the reaction rate without incurring a significant mass or parasitic power penalty. In this endeavor, lessons can be taken from the design of fuel cells to properly design the surrounding balance of plant as well as the design of the air cathode. Oxygen for the reaction can be obtained from either stored oxygen or ambient air. If the battery is lithium air, provision must be included in the design of the aircraft to gather sufficient air from the outside to feed the lithium-air reaction. This air may need to be pressurized, which will cost additional mass and parasitic power. It may also need to be dehumidified before it is introduced to the battery. This option may be the lightest system upon takeoff because no cathode reactants will have to be stored on the aircraft; however, as the flight continues, the battery will continually increase in weight, until it is recharged, at which point oxygen will be released. If the lithium-oxygen option is pursued, sufficient oxygen to maintain the reaction will need to be stored onboard the aircraft. This will include not only the oxygen but the tank(s) it will be stored in.

3.1.2 Possible Improvements to Batteries

The following subsections describe possible improvements for each type of lithium battery.

3.1.2.1 Improvements to Lithium-Ion Batteries

Anodes have generally been composed of graphite; however, work has begun to look at replacing graphite with lithium alloys of tin or silicon. These have significantly higher capacities than graphite, but they cannot as yet maintain their capacity during cycling. Ideally, pure lithium would be used for the anode; however, significant obstacles to cycling lithium anodes exist, including maintaining contact with the electrolyte surface, eliminating voids, and preventing the growth of lithium dendrites. Electrolyte chemistry also is being investigated to improve the performance and safety of lithium-ion batteries. Efforts continue to maximize the ionic conductivity of the electrolyte, minimize the mass impact of the electrolyte within the cell, improve the stability of the electrolyte at higher voltages, and continue to improve the overall safety of the electrolyte. In addition, stable cathode materials with higher lithium ion storage capacities and higher voltages are needed to advance the overall performance of lithium-ion cells. As work continues in all of these areas, it can be expected that the cell-level performance will continue to improve from today's average of 150 Wh/kg, to approximately 400 Wh/kg within 15 years and to 450 Wh/kg within 30 years.

Batteries are made up of a number of individual cells, and the number and arrangement depend on the overall battery voltage and capacity required. The battery case encloses the cells, provides structure, thermal interface, and at times, compression of the cells. Integrating the battery cells within a battery requires electrical wiring and a battery controller within the case. Currently, the battery case, the wiring, and other associated components compose approximately 30 percent of the overall battery mass. As improvements in lightweight materials and alternative conductors (e.g., nanotubes) become

available, it is reasonable to expect that, 15 years out, the mass of the case and associated hardware could be reduced to 20 to 25 percent of the overall battery mass and that, within 30 years, the mass of the case and associated hardware could be further reduced to 15 to 20 percent of the overall battery mass.

3.1.2.2 Improvements to Lithium-Sulfur Batteries

As work continues in the development of electrolytes, anodes, and cathodes, we can expect that cell-level performance will improve to where it will enable a commercial product with a cell-level specific energy of approximately 500 Wh/kg within 15 years and 800 Wh/kg within 30 years. As the cells are incorporated within a battery, the battery structure may need to accommodate the dimension changes experienced within the cell as a result of changes in the anode and cathode during cycling. As a result, the battery structure may contribute more to the overall weight of the battery than is seen with lithium-ion batteries. Within 15 years, the battery structural mass could contribute an additional 30 percent of the overall battery mass. Thirty years out, that may drop to 20 to 25 percent of the overall battery mass.

3.1.2.3 Improvements to Lithium-Air Batteries

As with lithium-sulfur batteries, a considerable amount of work remains to develop stable electrolytes, anodes, and cathode structure for lithium-air batteries. As work continues in all of these areas, we can expect cell-level performance to continue to improve and enable a commercial product with a cell-level specific energy of approximately 600 Wh/kg within 15 years and 1200 Wh/kg within 30 years.

Incorporating lithium-air cells within a battery may be a more complicated endeavor. In addition to the normal design problems with incorporating the cells into a battery, the design must provide air or oxygen to each cell of the battery and must maintain adequate and equal air or oxygen to each cell to maintain balance across the battery. Because of this design constraint, we expect that the mass penalty of moving from a cell to battery will be larger than for the other systems. Also, the air-handling system and the compressor system required at high altitude might add more weight to the system.

Lithium-air batteries designed within 15 years might have a battery-integration mass penalty of approximately 40 percent. Within 30 years, as materials continue to improve, the mass penalty could drop to 25 to 30 percent.

3.1.3 System Benefits of Improved Batteries

The following subsections describe the system benefits for each type of lithium battery.

3.1.3.1 System Benefits of Lithium-Ion Batteries

With potential future improvements in cell performance and materials in mind, a predicted battery mass sufficient to provide power for all phases of the reference mission was calculated for both the 1- and 10-MW electric motors using lithium-ion batteries (Figs. 43 and 44).

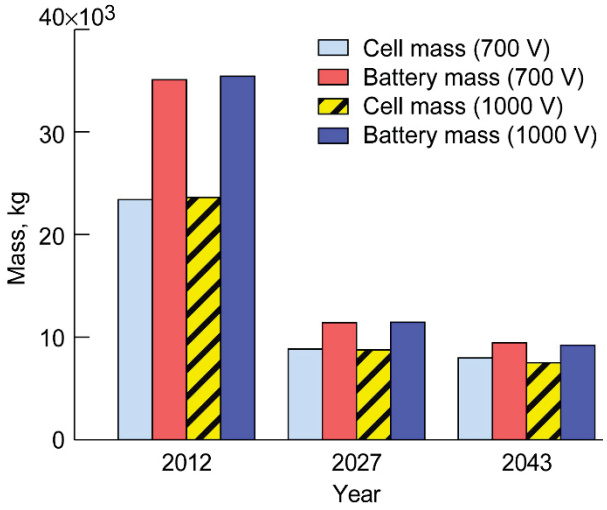

Figure 43.—Lithium-ion battery mass to provide power to the 1-MW electric motor model flight; 95-percent-efficient motor, 97-percent-efficient inverter, and 90-percent battery depth of discharge.

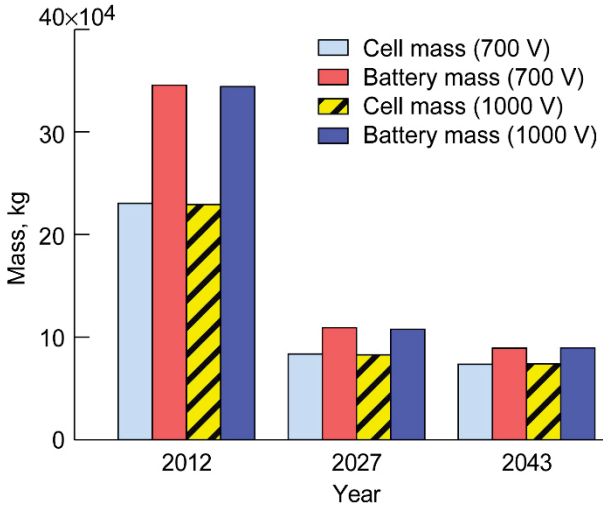

Figure 44.—Lithium-ion battery mass to provide power to the 10-MW electric motor model flight; 95-percent-efficient motor, 97-percent-efficient inverter, and 90-percent battery depth of discharge.

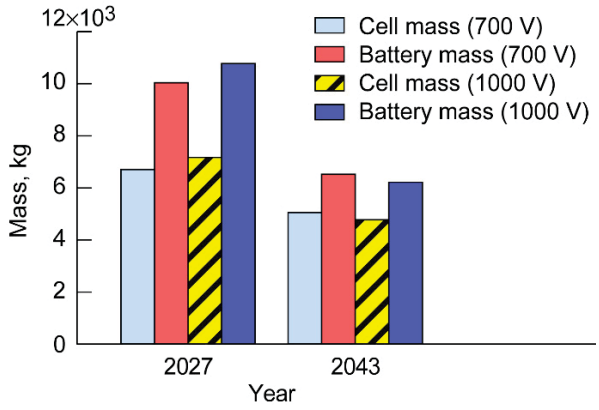

Figure 45.—Lithium-sulfur battery mass to provide power to a 1-MW electric motor; 95-percent-efficient motor, 97-percent-efficient inverter, and 90-percent battery depth of discharge. Lithium-sulfur cells are not currently available commercially.

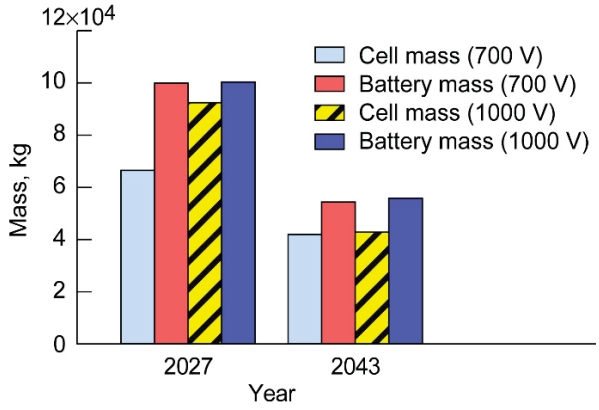

Figure 46.—Lithium-sulfur battery mass to provide power to a 10-MW electric motor; 95-percent-efficient motor, 97-percent-efficient inverter, and 90-percent battery depth of discharge. Lithium-sulfur cells are not currently available commercially.

As shown in the figures, the potential improvement within the next 15 to 30 years will enable substantial weight savings for the battery system to meet the power and energy needed by aircraft. Battery masses for both the 700- and 1000-V electrical bus cases also were calculated for each power level. As can be seen, the mass differences of the two cases are relatively small. Although the overall power and capacity needed is the same for both electrical buses, the nominal voltage that the battery is expected to deliver is different. Individual cells are arranged in a series configuration to meet the voltage required from the battery, and additional strings of series-wired cells are arranged in parallel within the battery to meet the current draw requirement and capacity. For a higher voltage to be delivered, more cells must be wired in series, and those series banks must be added to meet power and capacity demands. As additional strings containing large numbers of cells are added, they may overshoot power and capacity needs and result in a heavier battery.

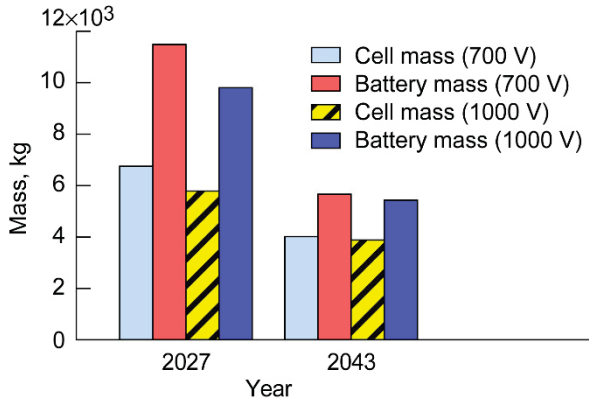

Figure 47.—Lithium air/oxygen battery mass to provide power to the 1-MW electric motor model flight; 95-percent-efficient motor, 97-percent-efficient inverter, and 90-percent battery depth of discharge. Lithium-air cells are not currently available commercially.

3.1.3.2 System Benefits of Lithium-Sulfur Batteries

Lithium-sulfur batteries are still a relatively immature technology. Assuming that the current barriers to commercially available lithium-sulfur are adequately addressed with continued improvements in cell performance and materials, predicted battery masses sufficient to provide power for all phases of the reference mission were calculated for both 1- and 10-MW electric motors (see Figs. 45 and 46).

A battery weight was not included for the current year, because no commercial lithium-sulfur cell has been developed that can sustain multiple charge/discharge cycles. As seen for the lithium-ion case, substantial weight savings can be expected with the improvement of the battery's specific capacity.

3.1.3.3 System Benefits of Lithium-Air Batteries

Lithium-air batteries, like lithium-sulfur batteries, are still at a low level of development for commercial use. Again, no battery weights were included for the current year's technology because a commercial product capable of multiple cycles is not yet available. With the potential future improvements in cell performance and materials in mind, a predicted battery mass sufficient to provide power for all phases of the reference mission was calculated for both 1- and 10-MW electric motors (see Figs. 47 and 48).

The battery masses for both the 700- and 1000-V electrical bus cases were calculated for each power level. As for the lithium-ion and lithium-sulfur battery projections, there are relatively small mass differences between the two cases. The overall arrangement of cells to meet both system bus voltage

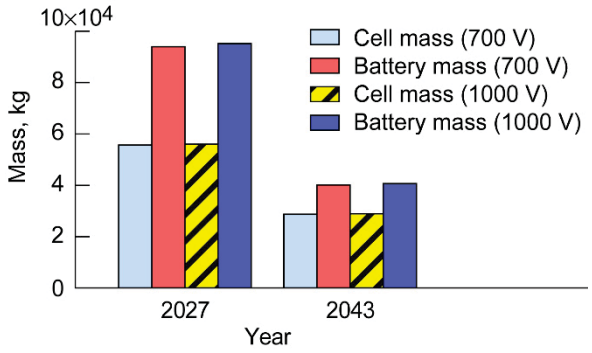

Figure 48.—Lithium-air/oxygen battery mass to provide power to the 10-MW electric motor model flight; 95-percent-efficient motor, 97-percent-efficient inverter, and 90-percent battery depth of discharge. Lithium-air cells are not currently available commercially.

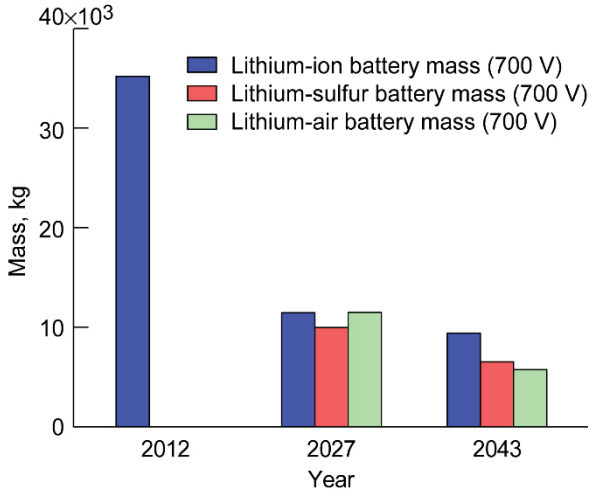

Figure 49.—Comparison of the three lithium battery chemistries under consideration to provide power to a 1-MW motor operating at 700 V; 95-percent-efficient motor, 97-percent-efficient inverter, and 90-percent battery depth of discharge.

and capacity can result in differences in mass for the different bus voltages.

3.1.3.4 Technology Comparison of Battery Types

Figure 49 shows the three battery technologies under consideration for the 1-MW electric motor with a 700-V system bus. As can be seen, with all three technologies, substantially lower battery masses are expected in the coming years. However, at 15 years out, the lithium-sulfur system is predicted to be 1000-kg lighter than either the lithium-ion or lithium-air battery system. After 30 years of development, the lithium-air/oxygen battery is expected to have the lowest battery mass. It is anticipated to be 1000-kg lighter than its nearest competitor, the lithium-sulfur battery.

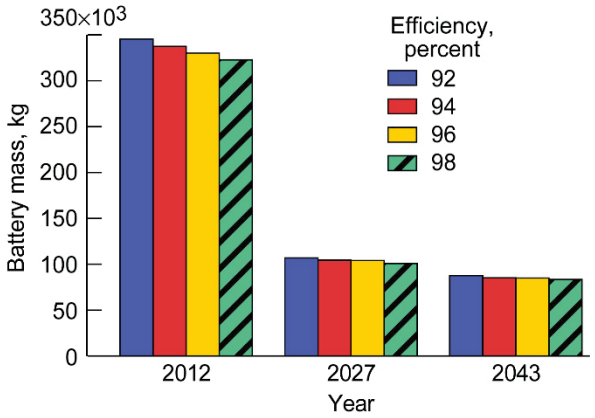

Figure 50.—Effect of system efficiency on the lithium-ion battery mass for a 10-MW electric motor operating at 700 V.

3.1.3.5 Effect of System Efficiency

Up to this point in the report, the battery weight assessments have assumed that the power demand of the overall propulsion system would remain the same within the projected 30-year period. However, in reality, it is likely that, with improved designs and materials, the power demands of an aircraft could drop substantially. A lower power demand will allow a smaller, lighter battery to be used. Another factor that is likely to change in the future is the overall system efficiency of the electric propulsion system. Specific system efficiencies were assumed for the calculation of the future battery mass for the reference flight. The two major players in system efficiency were assumed to be the electric motor and the inverter. It was assumed that the motor would be 95-percent efficient and that the inverter would be 97-percent efficient. Each percentage efficiency loss requires more power to be supplied from the source, that is, the battery. A larger power demand translates to a larger, heavier battery. Figure 50 shows the effect of improvements in the overall system efficiency on the battery weight. Higher efficiencies will translate to a lighter battery. For each percent improvement in efficiency, hundreds to thousands of kilograms of battery mass could be saved.

3.1.3.6 Rechargeability of Batteries

Just as a fuel tank must be refilled between flights, an energy storage system must be recharged. The choice and design of an energy storage system must take into account the time available before an aircraft must be used again, and the capability of the airport to provide the recharge power. Shorter recharge times would require a larger amount of power from the airport during recharging. The overall energy content provided to the energy storage system would be similar whether the system was recharged for 2 h or for 30 min, but the magnitude of the power necessary during the recharge would differ. One potential option for reducing recharge time without requiring large

quantities of power from an airport would be to swap out the energy conversion unit between flights. The "recharge time" with this process would be the time necessary to pull the spent system out, replace it with a new system, and perform whatever system checkouts are necessary. The spent system could be slowly recharged during off-peak electrical-use hours, saving the costs associated with electric power and improving charging efficiency by minimizing the waste heat produced when high recharge rates are used.

It also may be possible to provide some charging during the actual flight. Significant breakthroughs in the development of thin-film solar arrays have occurred in recent years. Solar array cells have been developed in the laboratory with a thickness on the order of a human hair. Also, work is underway to develop solar cell materials that could be painted onto a surface (Ref. 94). In the future, it may be possible to replace the paint on an aircraft with paint-on solar arrays. Power could be collected from both the top and bottom of the aircraft—the top collecting power from the incident sunlight, and the bottom collecting power from the light reflected off the ground. Approximately 1 kW/m^2 of sunlight reaches the ground under ideal conditions, and it has been projected that solar array efficiency could reach 30 to 40 percent in the future. With those developments, a considerable amount of extra power could be collected during and between flights. This power could be used to recharge the energy storage system to supply power during the flight rather than power from the energy storage system. An additional way to gather energy during flight could be to trade altitude for power during descent.

3.1.4 Summary of Battery Findings

Table 14 summarizes the potential benefits on a cell level. Although the battery-level improvements are ultimately what will be significant for the vehicle as a whole, the battery mass is a function of the mass of the cells and of all the other pieces making up the battery. As our understanding of batteries, designs, and materials continues to improve, it may be possible to move away from a conventional battery design and toward a battery more integral to the overall vehicle, allowing additional weight savings.

TABLE 14.—POTENTIAL IMPROVEMENTS IN CELL-LEVEL BATTERY PERFORMANCE

Battery	Cell-level specific energy, Wh/kg		
	State of the art	+15 years	+30 years
Lithium-ion	80 to 200	400	450
Lithium-sulfur	----------	500 to 650	800 to 950
Lithium-air	----------	600 to 750	1200 to 1400

3.1.5 Path Forward for Batteries

The predicted improvements in battery technology described here are contingent on continued research and development. The three battery technologies discussed hold considerable promise for future inclusion in hybrid electric aircraft systems. The cell-level projections for 15 years out have already been demonstrated in small laboratory cells, but significant work is still necessary to bring them to a practical working size. Continued development of anodes, cathodes, and electrolytes is necessary to reduce weight and improve performance, safety, and cycle life. The research and development currently underway in an effort to develop batteries for terrestrial electric vehicles could be leveraged, but the safety, performance, and weight goals for electric aircraft are likely to be beyond those for other electric vehicles. As materials and cell and battery designs continue to evolve, it may be possible to use some of the battery structure as part of the vehicle structure. Advances in the individual components of cells and overriding battery design may enable battery cells and batteries that can be conformed to fit the available space in an aircraft while being strong enough to become part of the aircraft support structure.

3.2 Flywheel Energy Storage

An energy source will be required to power the motor for either the hybrid electric or the turboelectric concept. This energy source is typically envisioned as a chemical battery; however, flywheels have many benefits for use in aircraft. These benefits include power densities that are an order of magnitude higher than those of chemical batteries with resultant fast charge and discharge times, low temperature sensitivity, long life, low maintenance, high depth of discharge, and low toxicity. They also have the potential added benefit of providing stabilized control for aircraft steering.

Flywheels store energy mechanically, in a spinning rotor. The flywheel is charged by speeding up the rotor and is discharged by slowing down the rotor, all through an integral motor/generator. These rotors achieve a high specific energy by using high-strength, low-density materials spinning at very high speeds. Figures 51 and 52 show a composite rim flywheel rotor built and tested at Glenn. The carbon fiber composite used in the rim has exceptionally high tensile strength, allowing the rotor to spin at up to 60 000 rpm. The rotor is enclosed in a vacuum tank and is levitated on magnetic bearings, resulting in very low losses and high efficiency.

Systems studies performed as part of the SUGAR Volt concept (Ref. 3) for hybrid electric and turboelectric aircraft have shown that the energy storage device needs to have a very high specific-energy density, on the order of 600 to 800 Wh/kg.

Figure 51.—Glenn's G2 flywheel rotor.

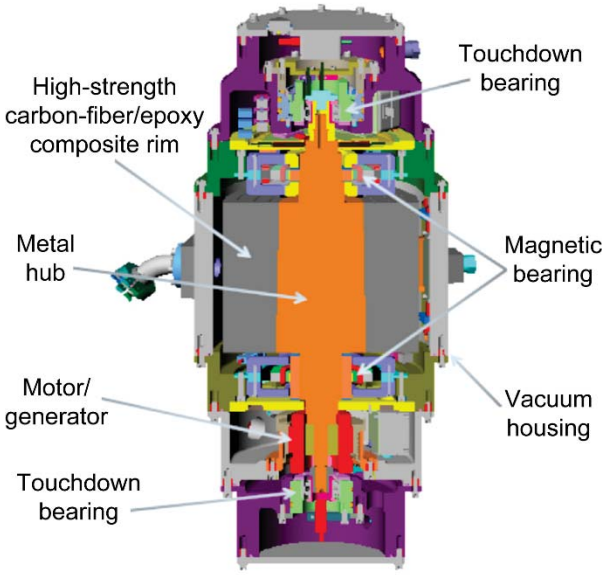

Figure 52.—Schematic of Glenn's flywheel.

Although battery technology is evolving rapidly, achieving such high energy densities will require considerable development. In addition, there are problems with temperature sensitivity in batteries, impacting efficiency, reliability, and life. High-specific-energy flywheels have the potential to achieve very high energy densities (Ref. 95) with low temperature sensitivity.

3.2.1 State of the Art of Flywheels

In 2008, Koh and Magee (Ref. 96) studied emerging energy-storage technologies, including various chemical battery types, capacitors, and flywheels. Although chemical batteries have the highest specific energies today, flywheels have a much higher gain in specific energy trend over time, and they look to overtake batteries in the coming years (Fig. 53). Currently, the specific energy of a flywheel rotor is about 100 Wh/kg. Assuming the same rate of increase, forecasting ahead 15 and 30 years indicates flywheel rotor specific energies approaching 1000 and 5000 Wh/kg, respectively.

The key parameter in determining the specific energy of a flywheel rim is the material's strength-to-density ratio, or S/ρ. The specific energy of the rim is directly proportional to this ratio and is defined for an isotropic material as

$$\frac{KE}{m} = \left(\frac{S}{\rho}\right)\left[\frac{(r_i/r_o)^2 + 1}{(3+\nu)+(1-\nu)(r_i/r_o)^2}\right] \tag{5}$$

where KE is the kinetic energy, m is the mass, r_i and r_o are the inner and outer radii of the cylindrical rim, and ν is Poisson's ratio. From Equation (5), we see that maximizing the strength-to-density ratio (specific strength) of the rim material will maximize the specific energy. Table 15 shows some specific

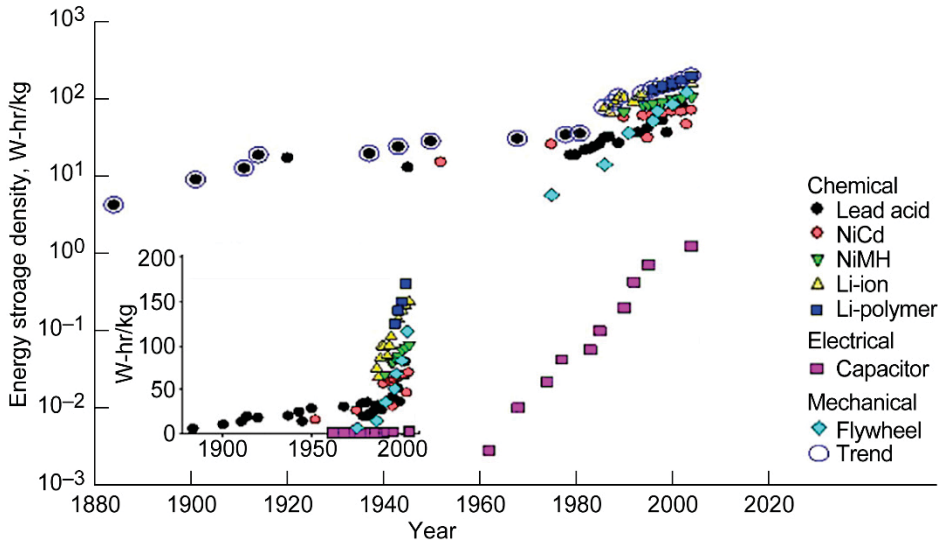

Figure 53.—Energy storage trends (Ref. 96). Reprinted from Technol. Forecast. Soc. Change, vol. 75, Koh, Heebyung; and Magee, Christopher L., A Functional Approach for Studying Technological Progress: Extension to Energy Technology, pp. 735–758, Copyright 2008, with permission from Elsevier.

TABLE 15.—SPECIFIC TENSILE STRENGTH AND RIM SPECIFIC ENERGY
[r_i/r_o = 0.7.]

Material	Derated specific tensile strength, kN-m/kg	Rim specific energy, Wh/kg
200-GPa nanofiber (predicted)	30 400	3430
100-GPa nanofiber (predicted)	15 200	1720
50-GPa nanofiber (predicted)	7 600	860
Carbon fiber with nanotubes (predicted)	1 940	220
Carbon fiber	970	110
Aramid	390	44
E-Glass with nanotubes	600	68
E-Glass	300	34

TABLE 16.—POWER AND ENERGY REQUIREMENTS FOR FLYWHEEL ENERGY STORAGE

Motor power class, MW	Flywheel power required, kW	Flywheel energy required, kWh	Charge/discharge time, h
1	1 082	2 947	2.7
10	10 815	29 471	2.7

strength values for various composite materials. Today, the highest strength material used in flywheels is carbon fiber composite, with a derated S/ρ of nearly 1000 kN-m/kg. For r_i/r_o = 0.7, the specific energy is 110 Wh/kg. As new high-strength materials are developed, specifically nanomaterials, this value will increase. A composite with 50-GPa nanofibers will yield a specific energy of 860 Wh/kg, similar to the projected value for 15 years from Figure 53. A composite incorporating 200-GPa nanofibers will yield a specific energy of 3430 Wh/kg, expected in about 30 years.

The specific energy of the flywheel module will be lower than that of the rim itself because of the added weights of other components, including the hub, flywheel motor, magnetic bearings, touchdown bearings, and housing. The weights of these components will depend on the power and energy, which are shown in Table 16 for the 1- and 10-MW systems (adapted from Table 13). The charge/discharge time is the ratio of the energy to the power.

As an example, the flywheel described by Strasik (Ref. 95) has a module specific energy of 38 Wh/kg, with an energy of 5 kWh, power of 3 kW, and a total weight of 132 kg. This flywheel utilizes a carbon-fiber-composite rim, which from Table 15, should have an approximate specific energy of 110 Wh/kg. Thus the rim mass should be about 46 kg, and other component masses should be about 86 kg. This particular flywheel is ground based, not optimized for low weight, and there will be opportunities to remove weight from the flywheel module. For example, using Kascak's equations (Ref. 97) for today's technology indicates that the specific energy of a 5-kWh, 3-kW flywheel module could be as high as 50 Wh/kg. On the basis of those equations and today's carbon-fiber-composite rotor, the 1-MW flywheel module investigated here should approach 80 Wh/kg. Kascak also shows that, as the flywheel energy gets larger, the flywheel module specific energy approaches the rotor specific energy.

The rotor size will clearly depend on the flywheel energy required. For example, for today's carbon-fiber-composite material, the flywheel rotor mass would be approximately 33 300 kg/MW. This mass would be reduced to 970 kg/MW in 30 years, assuming a composite material with 200-GPa fibers.

The motor size depends on the power and the discharge time. A very fast discharge time requires a much larger motor. For example, the Strasik flywheel has a discharge time of 1.7 h, which is lower than for the aircraft application (which has a relatively larger motor). For the 2.7-h discharge time, the motor mass would be less than 5 percent of the rotor weight for the carbon-fiber-composite rotor. For the same power level, this motor size would stay the same regardless of the rotor size.

The touchdown bearings would be sized to take the radial and axial loads of the flywheel in case of a power failure or sudden extreme load. Axially, the loads would be smaller for the lighter flywheel. However, the radial loads would be proportional to the rotor energy. Each rotor would have a slight unbalance proportional to the rotor weight, and the unbalance excitation force would be proportional to the square of the rotor speed. However, the touchdown bearing mass would be just a small percentage of the total flywheel module mass.

The majority of the added mass would come from the housing. The housing size depends on the size of the flywheel, scaling by area rather than volume. Therefore, the ratio of the

housing mass to the flywheel weight decreases with increasing rotor size. The power and energy required for aircraft is much higher than for the flywheels built and tested to date. Ground-based flywheels typically use a metal housing, often steel, so the mass is very high. Using high-specific-strength composites for the vacuum housing would significantly reduce the housing mass in comparison to today's technology.

For component and housing mass predictions, we assumed, for simplicity, that 10 percent of the component and housing mass would remain the same over the next 30 years and that the rest would scale with the rotor mass.

3.2.2 Possible Improvements to Flywheels

For a carbon-fiber-composite rim, today's expected flywheel specific energy is 110 Wh/kg. Assuming 95-percent efficiency and 90-percent depth of discharge, the flywheel module specific energy is 80 Wh/kg. For a 1-MW system, the rotor mass is approximately 33 300 kg, and the mass of the other components (motor, housing, etc.) is about 12 100 kg, which is an additional 36 percent over the rotor weight.

In 15 years, we expect that the use of 50-GPa fibers in composites will reduce the weight of the rotor. The expected flywheel specific energy will be 860 Wh/kg, giving a 3970-kg flywheel with 98-percent efficiency and 90-percent depth of discharge. The component and housing mass is assumed to be 2500 kg, giving a flywheel module specific energy of 450 Wh/kg.

Finally, in 30 years, we expect that 200-GPa fibers will be used in the composite rim, giving a flywheel specific energy of 3430 Wh/kg. For 99-percent efficiency and 90-percent depth of discharge, the rotor mass will be 970 kg, and the expected component mass will be 1520 kg, giving a flywheel module specific energy of 1180 Wh/kg.

3.2.3 System Benefits of Flywheels

Reducing the weight of the energy storage system will directly increase the horsepower per pound achieved by the entire propulsion system.

Table 17 summarizes the future specific energy benefits expected for the flywheel rim only as well as for the full flywheel module both now and in 15 and 30 years.

TABLE 17.—BENEFIT SUMMARY FOR FLYWHEEL ENERGY STORAGE

Component	Specific energy, Wh/kg		
	State of the art	+15 years	+30 years
Flywheel rim	110	860	3430
Flywheel module	80	450	1180

3.2.4 Path Forward for Flywheels

Several technologies need to be investigated to achieve the high specific-energy densities required for this application, including high-specific-strength rotor materials, flywheel motor technology, and reducing component masses. The first-order factor in flywheel specific energy is the rotor material strength-to-density ratio. Glenn has been investigating composite materials for high strength and low cost. Additional work needs to be done to mature carbon-fiber and nanotube material technology such that it can be utilized within a flywheel rotor system. Small batches of fiber need to be produced with consistent properties. Strength, fatigue, creep, and environmental effects need to be characterized. The best material system needs to be brought up to production levels, prototype flywheel rotors need to be made using the new fiber, and this work needs to be continued over time to achieve stronger and stronger rotor materials.

Safety is an important consideration for any type of energy storage device. NASA was involved for several years with a rotor safe-life program in cooperation with the University of Texas Center for Electromechanics. Composite flywheel rotors were tested to make sure that they had a safe failure mode, in which the rim underwent a noncatastrophic failure. The Defense Advanced Research Projects Agency (DARPA) also has a flywheel safety program that is looking at failure modes and detection. Proper flywheel design in coordination with monitoring will enhance the safety of flywheels. It is advisable to continue research and testing to ensure the safety of flywheels with reasonably sized containment for use in aircraft.

The most efficient flywheel would be one in which all the energy and mass were in the rotating mass. However, there are weights associated with the motor, magnetic bearings, and housing, in addition to other components. One means of reducing motor and magnetic bearing mass is a high-speed inside-out bearingless motor currently being developed at Glenn. This combination motor/magnetic bearing reduces weight in comparison to motors with individual components. The fact that it is inside out reduces the rotor hub size, concentrating more of the rotating energy out on the rim, increasing efficiency, and reducing weight. However, this technology is relatively new and has only been tested at low speed. Continued research in this area would go toward improving the specific energy of the flywheel, making it a viable candidate for energy storage in more-electric aircraft.

3.3 Supercapacitors

A third type of energy storage device that might be incorporated into hybrid electric propulsion is the supercapacitor, also known as the ultracapacitor. Like

traditional capacitors, the supercapacitor has very high power density, so it can charge and discharge rapidly. This may be of use when short-term high power is required, such as during takeoff, or for other power requirements such as providing power to electromechanical actuators. Currently, supercapacitors are used as backup power for Airbus 380 emergency exits. A disadvantage of traditional capacitors is their low energy density. However, supercapacitors have orders of magnitude higher energy density than traditional capacitors, bridging the gap between capacitors and batteries, as shown Figure 39. Other advantages of supercapacitors include a long cycle life (millions of charge/discharge cycles), good performance over a wide temperature range, high efficiency, and low toxicity. It may be that supercapacitors could be used along with another type of energy storage to optimally handle the requirements of hybrid electric propulsion, for example to decrease battery size and increase battery life.

A traditional capacitor consists of a pair of electrodes separated by an insulating dielectric material. When a voltage is applied to the capacitor, positive charge accumulates on one electrode, and negative charge accumulates on the other electrode. Energy is stored within the electric field between the electrodes. The capacitance is the ratio of the stored positive charge to the applied voltage. The energy E stored in a capacitor is directly proportional to the capacitance and is given by

$$E = \frac{1}{2} C V^2 \tag{6}$$

where C is the capacitance and V is the applied voltage. Therefore, increasing the capacitance or the voltage will increase the stored energy. The capacitance is related to the capacitor geometry and material properties through the relation

$$C = \varepsilon_o \varepsilon_r \frac{s}{x} \tag{7}$$

where ε_o is the permittivity of free space, ε_r is the dielectric constant of the insulating material, s is the surface area of the electrode, and x is the distance between electrodes. Clearly, the capacitance can be maximized by increasing the dielectric constant, increasing the electrode area, or decreasing the distance between electrodes. Supercapacitors achieve higher capacitance by doing just that.

The power calculation comes from assuming that the capacitor is in series with an external load resistance. The maximum power is then inversely proportional to the equivalent series resistance (ESR) of the capacitor, which includes the effects of components such as the electrodes and dielectric material. Keeping the ESR low ensures high power capability.

3.3.1 State of the Art of Supercapacitors

There are three kinds of supercapacitors: electrochemical double-layer capacitors (EDLCs), pseudocapacitors, and hybrid capacitors. Table 18, based on Burke (Ref. 98), shows the cell voltage, power density, and energy density of each type, assuming active mass (not total mass).

The EDLC consists of two electrodes in contact with an electrolyte solution, separated by a semipermeable membrane. Like the traditional capacitor, the charge storage is physical, not chemical. The membrane allows the ions to pass through while preventing shorting across the electrodes. The storage of charge is reversible, and the cycle life can be as high as 10^6 cycles (Ref. 99). The electrodes are made of advanced materials with very high surface area, for example a porous material such as activated carbon. New electrode materials are being investigated, including single-walled CNTs, which have high conductivity and high molecular surface area, and graphene sheets, where all the atoms are at the surface, maximizing the molecular surface area.

In a pseudocapacitor, energy storage occurs with charge transfer between the electrode and the electrolyte, where the ions in the solution combine with the electrode surface atoms (chemical charge storage). The electrode material is typically a metal oxide or a conducting polymer, which have high conductance, low ESR, and high capacitance. One metal oxide material being studied is ruthenium oxide (RuO_2), but its cost is relatively high (Ref. 99). Another is manganese dioxide (MnO_2), which is cheaper but has lower electrical conductivity (Ref. 100). A drawback of conducting polymers is lower cycle life. These devices are not yet commercially available.

TABLE 18.—PROPERTIES OF SUPERCAPACITORS
[Adapted from Ref. 98.]

Supercapacitor type	Cell voltages, V	Power density, kW/kg	Energy density, Wh/kg
Electrochemical double-layer	2.5 to 3.5	1 to 3	5 to 12
Pseudocapacitor	2 to 3.5	1 to 2	10 to 15
Hybrid	1.5 to 3.3	1 to 2	10 to 15

A hybrid capacitor is a combination of an EDLC and a pseudocapacitor. The three types of hybrid supercapacitors being studied are composite, symmetric, and battery supercapacitors (Ref. 99). Composite hybrid supercapacitors combine both chemical and physical charge storage in each electrode. Asymmetric supercapacitors include an EDLC electrode and a pseudocapacitor electrode. Finally, battery supercapacitors combine a supercapacitor electrode with a battery electrode. Like pseudocapacitors, hybrid capacitors are not yet available commercially.

3.3.2 Possible Improvements to Supercapacitors

Halper and Ellenbogen (Ref. 99) discuss several areas of research for supercapacitors. One area is the hybrid supercapacitor, which incorporates the benefits of both EDLCs and pseudocapacitors and allows the hybrid supercapacitor to outperform both. Other research areas include decreasing the ESR of supercapacitors (increasing power density), optimizing the electrolyte or dielectric material (increasing power density and energy density), and reducing the tendency of supercapacitors to self-discharge (affecting performance).

Chen et al. (Ref. 100) report on a hybrid supercapacitor using nanostructured MnO_2 and CNTs with commercially available sponge as the substrate (Fig. 54). The sponge naturally has very high porosity, is lightweight, and allows for continuous coating of CNTs. This device achieved a power density of 63 kW/kg and an energy density of 31 Wh/kg, based on active mass.

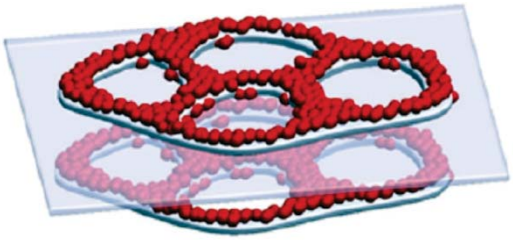

Figure 54.—MnO_2-carbon nanotube sponge supercapacitor (Ref. 100). Reprinted with permission from Chen, Wei, et al.: High-Performance Nanostructured Supercapacitors on a Sponge. Nano Lett., vol. 11, 2011, pp. 5165–5172. Copyright 2011, American Chemical Society.

To improve the surface area of EDLC electrodes, Liu et al. (Ref. 101) used curved graphene sheets in the electrode. Graphene sheets have high conductivity and are a single atom thick so the surface area is already quite high. Adding folds to these sheets increases the surface area considerably and also keeps the sheets from restacking, which can decrease the effective surface area. This configuration reached an energy density of 85.6 Wh/kg at room temperature with a power density of approximately 0.6 kW/kg and a discharge time of 580 s. An energy density of 53.1 Wh/kg was achieved with a power density of 9.8 kW/kg and a discharge time of 20 s. The energy and power density values were based on active mass.

Lin et al. (Ref. 102) describe another method of optimizing the surface area of graphene sheets for EDLC electrodes. They deposited silver nanoparticles onto the graphene sheets, then heated those graphene sheets in air. The silver nanoparticles were oxidized into gaseous byproducts, and then the silver was removed. This left holes in the graphene surface that were on the order of about five to tens of nanometers in diameter.

Wang et al. (Ref. 103) discuss supercapacitor electrode materials with tuned porosity that are fabricated from paper-pulp-mill sludge biowaste—a low-cost waste material that would otherwise be incinerated or put in landfills. With this material, they achieved 51 Wh/kg at 375 W/kg, and 26 to 31 Wh/kg at 6760 to 7000 W/kg. It is important to note that, like other energy storage devices, the energy density and power density can be defined in different ways. These reported values include only the active material weight. Wang states that carbon weight accounts for about 30 percent of the total mass of packaged superconductors. They expect to achieve a practical energy density of 15 Wh/kg for a packaged device, an improvement of 3 times over the state of the art.

3.3.3 Benefit Summary of Supercapacitor Improvements

Both the power density and energy density of supercapacitors should increase with new material improvements in electrode and dielectric materials and with the development of new hybrid supercapacitors. Table 19 details the benefits expected in 15 and 30 years.

TABLE 19.—SUPERCAPACITOR BENEFIT SUMMARY

Property	State of the art	+15 years	+30 years
Energy density (active mass), Wh/kg	5 to 15	100 to 150	200 to 300
Power density (active mass), kW/kg	1 to 3	2 to 3	4 to 6

4.0 Related Research on System Modeling

Research is ongoing to determine the benefits of hybrid electric and turboelectric aircraft from a systems perspective as well as to investigate the electrical distribution system. The systems-level research will help to define the motor requirements (e.g., efficiency and power density) for a particular aircraft and configuration and also will estimate the decreases in noise, emissions, and fuel burn. Glenn is involved with the SUGAR program as part of a collaborative effort among several companies and institutions, including Boeing Research and Technology, Georgia Institute of Technology, and Virginia Polytechnic Institute and State University. As an example, the systems analysis of the N+3 SUGAR Volt concept, a ~150-passenger aircraft with hybrid-electric propulsion, incorporated various levels of energy density to predict fuel-burn benefits. A 8000-hp motor/generator at 2 to 3 hp/lb coupled with a 750-Wh/kg battery gave a reduction in fuel burn of about 60 percent (Ref. 3).

Several studies are also ongoing with regard to the electrical distribution system. The use of hybrid electric or turboelectric propulsion will create electrical loads that are unprecedented in commercial aircraft. A traditional electrical distribution system will not be able to supply the large power loads created by the motors; therefore, a new system must be contrived. Because of the highly integrated nature of electrical systems, their design is highly dependent on the performance of each component. Because the motors will be the largest load on the system, the motor type and performance will have a discernible impact on the electrical distribution system. In order to study the effects of advancements in motor technologies, a modeling and simulation environment is being created that can optimize the electrical distribution system for a given motor design. This optimization aims to find the lightest and most efficient system possible while maintaining stability and reliability. Studies have shown that, using a system-level optimization routing, a 5-percent weight savings can be achieved (Ref. 104).

An example of the electric distribution system modeling is the sizing of the transmission cables performed by Angela Lowe at Georgia Tech as part of NASA's Graduate Student Research Program. In this case study, the cable configuration used included a cylindrical copper core, dielectric layer, magnetic shield, and cooling sleeve. Calculation of the size of cable needed was based on the power demand of the load, power losses through the cable, system nominal voltage, and allowable heat rejection from the cable. As technologies change and loads vary, the model could be updated with new parameters to show how a technology impacts the size of the cable. Figures 55 and 56 show an example of the results produced by the model. For the model to produce these results, the power load was set to 40 MW so that it was representative of the loads found on the NASA N3–X (Ref. 74). The allowable heat rejection from the cable was set to 0.2 percent of the power load based on the study in Reference 105. Figure 55 shows the cable diameter as a function of system nominal voltage and cable length, and Figure 56 shows the cable weight. The data in the curves can be regressed to provide a function that can predict the size of the cables based on voltage and length. Later this information can be used in the optimization routine to determine what system nominal voltages are appropriate for the system and what technology advances are needed to reach a reasonable cable size. For the study in this report, we can see the difference in the weight of cable for today's 120-V system versus a 700- or 1000-V system in the future.

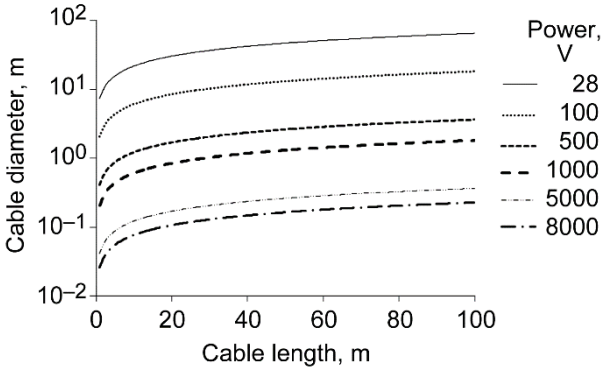

Figure 55.—Room temperature cable diameter.

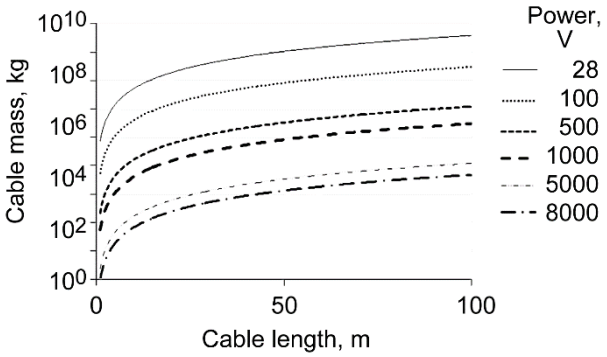

Figure 56.—Room temperature cable weight.

Another study was completed by Rolls Royce under contract to NASA to model and characterize high-power electrical systems for turboelectric aircraft. This system included two turboshaft engines, which provided power for a bank of fans located at the trailing edge of the aircraft. Superconducting generators and motors were included, along with flywheels as energy storage. This study generated system architecture recommendations and produced a dynamic system model, the results of which are included in the contractor report, "Stability, Transient Response, Control, and Safety of a High-Power Electric Grid for Turboelectric Propulsion of Aircraft" (Ref. 106).

Another study of the electrical distribution system was done by Georgia Tech as part of the SUGAR Volt project. Using the Numerical Propulsion System Simulation (NPSS) system modeling code that was originally designed at NASA, Georgia Tech is developing the electrical transmission and distribution system, including the inverter, rectifier, DC transformer, generator, motor, bus, and energy storage device.

Glenn has also built a Propulsion Electric Grid Simulator, which represents a turboelectric propulsion system through the use of motors, generators, electric bus, and control system. This test setup enables rapid analysis and demonstration of a system-level proof-of-concept for the electrical distribution system.

The information gained using aircraft systems analysis and electrical distribution system optimization could aid in the realization of a room temperature hybrid or turboelectric propulsion system by producing a lightweight, stable, and reliable design. The system-level optimization process could produce significant weight savings and increase efficiency. As the technologies for room temperature motors and power electronics progress, the models could be updated with new performance parameters. Lastly, this information could be used to determine which technology improvements have the greatest impact on the system.

5.0 Technology Assessment Conclusion

The Subsonic Fixed Wing Project of the Fundamental Aeronautics Program is researching aircraft propulsion technologies that will lower noise, emissions, and fuel burn. This study was initiated to evaluate the possibility of using noncryogenic electric motors as part of an electric propulsion system that would provide benefits in all of these categories without incurring the added risk of developing flightworthy cryogenic systems.

The technology improvements that were investigated in this study include motor-related technologies, energy-storage-related technologies, and system modeling approaches. Motor efficiency and power density could be improved through the use of better conductors, insulators, magnets, bearings, structural materials, and thermal management. Energy storage could be improved through batteries, flywheels, or supercapacitors, all of which expect significant energy density improvements over the next few decades.

The benefits shown in this study are quite significant. The technology improvements described may bridge the gap in power density and efficiency between currently available off-the-shelf motors, electronics, and energy storage components and the projected cryogenically cooled superconducting motor technology.

Table 20 summarizes the projected benefits due to each technology in 15 and 30 years. These improvements will only be realized if there is continued research and support coupled with a consistent desire to achieve NASA's Fundamental Aeronautics goals of reducing fuel burn, emissions, and noise, thereby minimizing the environmental impact of aviation.

Glenn Research Center
National Aeronautics and Space Administration
Cleveland, Ohio, January 20, 2015

TABLE 20.—SUMMARY OF EXPECTED TECHNOLOGY IMPROVEMENTS

Technology or electrical component	State of the art	+15 years	+30 years
Electric motor—all technologies			
Energy density, hp/lb	3	8	16
Power electronics			
Energy density, hp/lb	5	6	7
Efficiency, percent	93 to 95	98	99
Energy storage (based on active mass only)—specific energy, Wh/kg			
Lithium-ion batteries (cell only)	80 to 200	400	450
Lithium-sulfur batteries (cell only)	----------	500 to 650	800 to 950
Lithium-air batteries (cell only)	----------	600 to 750	1200 to 1400
Flywheels (rim only)	110	860	3430
Supercapacitors (active mass only)	5 to 15	100 to 150	200 to 300

References

1. Brown, Gerald V.: Efficient Flight-Weight Electric Systems. Presented at the Fifth Fundamental Aeronautics Program Technical Conference, Cleveland, OH, 2012.
2. N+2 Electric Distributed Propulsion Aircraft for Terminal Area Operations. ESAero, Pismo Beach, CA. http://esaero.com/ Accessed Dec. 2, 2013.
3. Bradley, Marty K.; and Droney, Christopher K.: Subsonic Ultra Green Aircraft Research: Phase I Final Report. NASA/CR—2011-216847, 2011. http://ntrs.nasa.gov/
4. Arpingstone: Lufthansa. http://en.wikipedia.org/wiki/File:Lufthansa-1.jpg Accessed Dec. 2, 2013.
5. CFM56–3 Aero Engine Maintenance Training Center, 2005. http://218.6.160.223/eng/prod01.htm Accessed Dec. 2, 2013.
6. PT–LUZ. http://www.jetphotos.net/viewphoto.php?id=6807140 Accessed Dec. 2, 2013.
7. CJ610. U.S. Turbine & Accessory, LLC, 2013. http://www.usturbine.us/cj610.html Accessed Nov. 12, 2014.
8. Buress, T.A., et al.: Evaluation of the 2010 Toyota Prius Hybrid Synergy Drive System. ORNL/TM–2010/253, 2010.
9. YASA Motors—Powering the Future. YASA Motors, Milton Park, Abingdon, 2013. http://www.yasamotors.com Accessed Dec. 2, 2013.
10. Launchpoint Technologies 6" Dual Halbach Air-Core Motor. Rev. 1.0, Launchpoint Technologies Inc. http://www.launchpnt.com/Portals/53140/docs/dual-halbach-motor-data-sheet_r1.pdf Accessed Dec. 2, 2013.
11. Kuznetsov, Stephen: Machine Design and Configuration of a 7000 HP Hybrid Electric Drive for Naval Ship Propulsion. 2011 IEEE International Electric Machines and Drives Conference (IEMDC), 2011, p. 1625.
12. Proven Power Dense Solution for Advanced Naval Propulsion. DRS Technologies, Arlington, VA, 2013. http://www.drs.com Accessed Dec. 2, 2013.
13. Huang, Surong, et al.: A General Approach to Sizing and Power Density Equations for Comparison of Electrical Machines. Research Report 96–16, IEEE–IAS Conf. Rec., 1996, pp. 836–842.
14. Nanotubes and Buckyball. Nanotechnology Now, 2012. http://www.nanotech-now.com/nanotube-buckyball-sites.htm Accessed July 7, 2012.
15. Carbon Nanotube. Wikipedia Foundation, San Francisco, CA, 2013. http://en.wikipedia.org/wiki/Carbon_nanotube Accessed July 7, 2012.
16. Carbon Nanotube Science and Technology. A Carbon Nanotube Page. University of Reading, UK, 2012. http://www.personal.reading.ac.uk/~scsharip/tubes.htm Accessed July 7, 2012.
17. Peng, Bei, et al.: Measurements of Near-Ultimate Strength for Multiwalled Carbon Nanotubes and Irradiation-Induced Crosslinking Improvements. Nature Nanotechnology, vol. 3, 2008, pp. 626–631. Accessed July 7, 2012.
18. Graphene. Wikipedia Foundation, San Francisco, CA, 2013. http://en.wikipedia.org/wiki/Graphene Accessed July 7, 2012.
19. Copper-Clad Aluminum. International Cablemakers Federation, Vienna, Austria. http://www.icf.at/en/6049/copper_clad_aluminium.html Accessed July 7, 2012.
20. Experiments With Magnets and Conductors. Magnet Man, 2013. http://www.coolmagnetman.com/magconda.htm Accessed July 7, 2012.
21. General Nano LLC. SBR/STTR, U.S. Government, Washington, DC. http://www.sbir.gov/sbirsearch/detail/172986 Accessed July 7, 2012.
22. The Strongest, Lightest and Most Conductive Material Known. Nanocomp Technologies, Inc., Merrimack, NH, 2012. http://www.nanocomptech.com/what-are-carbon-nanotubes.html Accessed July 7, 2012.
23. Zhao, Yao, et al.: Iodine Doped Carbon Nanotube Cables Exceeding Specific Electrical Conductivity of Metals. Sci. Reports, vol. 1, no. 83, 2011, pp. 1–5.
24. Behabtu, Natnael, et al.: Strong, Light, Multifunctional Fibers of Carbon Nanotubes With Ultrahigh Conductivity. Sci., vol. 339, no. 182, 2013, pp. 182–186.
25. Maxwell, James L.; Rose, Chris R.; and Ramos, Octavio, Jr.: Ultraconductus: Innovative Electrical Conductors. Los Alamos National Laboratory, Los Alamos, NM, 2011. http://www.lanl.gov/science/NSS/issue2_2011/story5full.shtml Accessed Dec. 2, 2013.
26. Magnet Wire Insulation Guide. MWS Wire Industries, Westlake Village, CA, 2011. http://www.mwswire.com/pdf_files/mws_tech_book/page2_3.pdf Accessed Dec. 2, 2013.
27. Hatano, Hiroshi: Development of High Thermal Conducting Insulation for Turbine Generator Stator Coil. EINA Magazine No. 13, 2006. http://eina.ws/no13/EINA_No13p41-42.pdf Accessed Dec. 2, 2013.
28. Kikuchi, Hideyuki; and Hanawa, Hidehito: Inverter Surge Resistant Enameled Wire With Nanocomposite Insulating Material. IEEE Trans. Dielec. Elect. Insul., vol. 19, no. 1, 2012, pp. 99–106.
29. DuPont Kapton Polyimide Film. DuPont publication H–38479–9, 2012.
30. PYRE-M.L. Wire Enamel. Industrial Summit Technology, Technical Bulletin #ML–1–95. http://www.istusa.com/pdf/Pyre-ML-Technical-Bulletin.pdf Accessed Jan. 14, 2015.
31. PEEK Insulated Wire. Zeus PEEK datasheet, Zeus, Inc., Orangeburg, SC. http://www.zeusinc.com/UserFiles/zeusinc/Documents/technical_salessheets/PEEK_InsulatedWire_ZEUS.pdf Accessed Dec. 2, 2013.
32. Poly(etheretherketone) (PEEK). ASM International, Materials Park, OH, 2013. http://www.asminternational.org/content/docs/PEEK.pdf Accessed Dec. 2, 2013.
33. Suzuki, Kazunori; Murouchi, Kengo; and Magari, Yukinobu: New Heat Resistant Magnet Wire: "Polyimide-Silica Hybrid Enameled Wire." Hitachi Cable Review, No. 20, 2001, pp. 91–96.

34. Zhi, Chunyi, et al.: Towards Thermoconductive, Electrically Insulating Polymeric Composites With Boron Nitride Nanotubes as Fillers. Adv. Func. Mater., vol. 19, 2009, pp. 1857–1862.
35. Li, Tung-L.; and Hsu, Steve Lien-Chung: Enhanced Thermal Conductivity of Polyimide Films Via a Hybrid of Micro- and Nano-Sized Boron Nitride. J. Phys. Chem. B, vol. 114, 2010, pp. 6825–6829.
36. Thompson, Marc T.: Practical Issues in the Use of NdFeB Permanent Magnets in Maglev, Motors, Bearings, and Eddy Current Brakes. Proc. IEEE, vol. 97, no. 11, 2009, p. 1758.
37. Constantinides, S.: The Magnetic Material Challenge. ARPA–E Workshop, Rare Earth and Critical Materials, Arlington, VA, 2010. http://www.arnoldmagnetics.com/Rare_Earth_Information.aspx Accessed Dec. 3, 2013.
38. Nanocomposite Magnets. GE Global Research, Department of Energy, Washington, DC, 2013. http://arpa-e.energy.gov/?q=arpa-e-projects/nanocomposite-magnets Accessed Dec. 3, 2013.
39. NEOMAX Magnet Product Catalog, Hitachi Metals, Ltd., Tokyo, Japan, 2013. http://www.hitachi-metals.co.jp/e/eh2009/data/NEOMAXCatalog2.pdf Accessed Dec. 2, 2013.
40. Matsuura, Yutaka: Recent Development of Nd-Fe-B Sintered Magnets and Their Applications. J. Magnetism Magnetic Mater., vol. 303, no. 2, 2006, pp. 344–347.
41. Electric Vehicle Propulsion. Launchpoint Technologies Website, Goleta, CA. http://www.launchpnt.com/portfolio/aerospace/uav-electric-propulsion/ Accessed Dec. 9, 2014
42. Coey, J.M.D.; and Skomski, Ralph: New Magnets From Interstitial Intermetallics. Research Papers in Physics and Astronomy (Physics Scripta, vol. T49, 1993, pp. 315–321), Paper 14, Ralph Skomski Publications, 1993. http://digitalcommons.unl.edu/cgi/viewcontent.cgi?article=1013&context=physicsskomski Accessed June 18, 2014.
43. Johnson, Francis: Transformational Nanostructured Permanent Magnets. Advanced Research Projects Agency, DOE. http://www.arpae-summit.com/em_reporting/exhibitor_detail?exhibitor_id=4497 Accessed Dec. 9, 2014
44. Hadjipanayis, G.C.: High-Energy Permanent Magnets for Hybrid Vehicles and Alternative Energy. University of Delaware, Newark, DE. http://www.arpae-summit.com/em_reporting/exhibitor_detail?exhibitor_id=4487 Accessed Aug. 12, 2014.
45. Hadjipanayis, George C.; and Xiao, John Q.: Novel Materials for High Energy and Power Density. University of Delaware Energy Institute Symposium, Newark, DE, 2008. http://www.energy.udel.edu/pdf/Hadjipanayis_UDEI_Symposium.pdf Accessed Dec. 3, 2013.
46. Liu, Jinfang: Sm-Co Magnets and Applications. Electron Energy Corporation, Landisville, PA. http://www.electronenergy.com/media/SmCo%20Magnets%20and%20Applications.pdf Accessed Dec. 3, 2013.
47. Gallego, Nidia C.; and Klett, James W.: Carbon Foams for Thermal Management. Carbon, vol. 41, 2003, pp. 1461–1466.
48. Shin, E. Eugene; Johnston, J. Chris; and Haas, Daniel: Advances in the Lightweight Air-Liquid Composite Heat Exchanger Development for Space Exploration Applications. AIAA 2011–5206, 2011.
49. Brown, Gerald V., et al.: Ultra-High-Power, Lightweight Cryogenic Motor Developed and Operated in Liquid Nitrogen. NASA/TM—2008-215054, 2008. http://ntrs.nasa.gov
50. Gieras, J.F.: Advancements in Electric Machines. Springer, New York, NY, 2008, p. 102.
51. Lawson, Craig P.; and Pointon, James M.: Thermal Management of Electromechanical Actuation on an All-Electric Aircraft. Proceedings of the 26th International Congress of the Aeronautical Sciences, Anchorage, AK, 2008.
52. Lowe, Angela: Aircraft Energy Architecture Modeling Evaluation: Thermal Management System. Presentation for the Georgia Institute of Technology, Aerospace Systems Design Laboratory (ASDL), Jan. 31, 2011.
53. Ohadi, M.; and Qi, J.: Thermal Management of Harsh-Environment Electronics. 20th IEE SEMI–THERM Symposium, 2004.
54. Filburn, Tom; Kloter, Amanda; and Cloud, Dave: Design of a Carbon-Carbon Finned Surface Heat Exchanger for a High-Bypass Ratio, High Speed Gas Turbine Engine. ASME GT2006–90480, 2006.
55. Chandler, David L.: Insulators Made Into Conductors. MIT News, 2010. http://web.mit.edu/newsoffice/2010/heat-nanofibers-0308.html Accessed Dec. 3, 2013.
56. Shen, Sheng, et al.: Polyethylene Nanofibers With Very High Thermal Conductivities. Nature Nanotech., vol. 5, 2010, pp. 251–255.
57. Jacobi, Anthony M., et al.: Novel Materials for Heat Exchangers. ARTI Report No. 06030–01, 2008.
58. Merritt, Bernard T., et al.: Halbach Array Motor/Generators—A Novel Generalized Electric Machine. Lawrence Livermore National Laboratory, UCRL–JC–119050, 1994.
59. Yu, Min-Feng, et al.: Strength and Breaking Mechanism of Multiwalled Carbon Nanotubes Under Tensile Load. Sci., vol. 287, 2000, pp. 637–640.
60. Collins, Philip G.: Nanotubes for Electronics. Sci. Amer., vol. 283, 2000, pp. 62–69.
61. Abu-Zahra, Esam H.: High Strength E-Glass/CNF Fibers Nanocomposite, Ph.D. Thesis, Cleveland State Univ., 2007.
62. Grimmer, Christopher S.; and Dharan, C.K.H.: High-Cycle Fatigue of Hybrid Carbon Nanotube/Glass Fiber/Polymer Composites. J. Mater. Sci., vol. 43, no. 13, 2008, pp. 4487–4492.
63. Provenza, Andrew J.: Stator and Rotor Designed and Manufactured for an Ironless High-Power-Density Permanent Magnet Electric Motor for Pollution-Free

Aircraft. Research and Technology 2005, NASA/TM—2006-214016, 2006, pp. 162–163. Available from the NASA Center for Aerospace Information.
64. ThinGap Motor Technologies, Ventura, CA, 2008. http://www.thingap.com/ironless-composite-stator/ Accessed Dec. 4, 2013.
65. Kascak, Albert F., et al.: Stability Limits of a PD Controller for a Flywheel Supported on Rigid Rotor and Magnetic Bearings. NASA/TM—2006-213979 (AIAA–2005–5956), 2006. http://ntrs.nasa.gov
66. Choi, Benjamin; and Siebert, Mark: A Cryogenic High-Power-Density Bearingless Motor for Future Electric Propulsion. NASA/TM—2008-215211, 2008. http://ntrs.nasa.gov
67. Ooshima, Masahide, et al.: Design and Analysis of Permanent Magnet-Type Bearingless Motors. IEEE Trans. Indus. Electr., vol. 43, no. 2, 1996, pp. 292–299.
68. Chiba, Akira, et al.: Stable Operation of Induction-Type Bearingless Motors Under Loaded Conditions. IEEE Trans. Ind. App., vol. 33, no. 4, 1997, pp. 919–924.
69. Ichikawa, O., et al.: A Decoupling Control Method of Radial Rotor Positions in Synchronous Reluctance Type Bearingless Motors. Proceedings of the 1995 International Power Electrical Conference. Vol. 1, 1995, pp. 346–351.
70. Takemoto, Masatsugu; Chiba, Akira; and Fukao, Tadashi: A Method of Determining Advanced Angle of Square-Wave Currents in Bearingless Switched Reluctance Motors. IEEE Trans. Ind. App., vol. 37, no. 6, 2001, pp. 1702–1709.
71. Gotzhein, Christina: Successful Maiden Flight of a Bearingless Advanced Technology Rotor Innovative Rotor Technology for Increased Comfort and Reduced Costs. Press Release, 2006. http://www.eurocopter.com/site/en/press/Successful-maiden-flight-of-a-bearingless-Advanced-Technology-Rotor-Innovative-rotor-technology-for-increased-comfort-and-reduced-costs_390.html?iframe=true&width=700 Accessed Dec. 4, 2013.
72. Choi, Benjamin; and Siebert, Mark: A Bearingless Switched-Reluctance Motor for High Specific Power Applications. NASA/TM—2006-214486 (AIAA–2006–4804), 2006. http://ntrs.nasa.gov
73. Technical presentation, NAVY MAG BEARING PAYOFFS. Naval Aviation Systems TEAM, Propulsion & Power Engineering.
74. Brown, Gerald V.: Weights and Efficiencies of Electric Components of a Turboelectric Aircraft Propulsion System. AIAA–2011–225, 2011.
75. Lightweight, Efficient Power Converters for Advanced Turboelectric Aircraft Propulsion Systems. Final Report, NASA 2010 Phase 1 SBIR, NNX10CC71P, MTECH Laboratories, LLC, Ballston Spa, NY, 2010.
76. 2011 Annual Progress Report: Advanced Power Electronics and Electric Motors. U.S. Department of Energy, Energy Efficiency and Renewable Energy, Vehicle Technologies Program, DOE/EE–0676, 2011. https://www1.eere.energy.gov/vehiclesandfuels/pdfs/program/2011_apeem_report.pdf. Accessed June 18, 2014.
77. Tolbert, Leon M., et al.: Impact of SiC Power Electronic Devices for Hybrid Electric Vehicles. SAE Technical Paper 2002–01–1904, 2002.
78. Full SiC Intelligent Power Module. Mitsubishi Electric, Tokyo, 2013. http://www.mitsubishielectric.com/company/environment/report/products/randd/sic/index.html Accessed Dec. 4, 2013.
79. Momota, Seiji; Hitoshi, Abe; and Horasawa, Takayasu: Plated Chip for Hybrid Vehicles. Fuji Electric Review, vol. 54, no. 2, 2008. http://www.fujielectric.com/company/tech/pdf/54-02/FER-54-02-049-2008.pdf
80. Kötz, R.; and Carlen, M.: Principles and Applications of Electrochemical Capacitors. Electrochimica Acta, vol. 45, no. 15, 2000, pp. 2483–2498.
81. A Technical Assessment of High-Energy Batteries for Light-Duty Electric Vehicles. Global Climate & Energy Project, Stanford University, Stanford, CA, 2006. http://gcep.stanford.edu/pdfs/assessments/ev_battery_assessment.pdf Accessed Dec. 5, 2013.
82. AA Portable Power Corp. www.batteryspace.com Accessed Dec. 5, 2013.
83. Duleep, Gopalakrishnan, et al.: Assessment of Electric Vehicle and Battery Technology. Delft, 2011.
84. Scrosati, Bruno; and Garche, Jurgen: Lithium Batteries: Status, Prospects and Future. J. Power Sources, vol. 195, 2010, pp. 2419–2430.
85. Sion Power: The Rechargeable Battery Company. http://sionpower.com/ Accessed Dec. 5, 2013.
86. Kolosnitsyn, V.S.; and Karaseva, E.V.: Lithium-Sulfur Batteries: Problems and Solutions. Russian J. Electrochem., vol. 44, no. 5, 2008.
87. Liang, C., et al.: Challenges and Solutions for Lithium-Sulfur Batteries. Presented at the 2011 U.S.-China Electric Vehicle and Battery Technology Workshop, 2011.
88. Zhang, Y., et al.: Development in Lithium/Sulfur Secondary Batteries. Open Mater. Sci. J., vol. 5 (Suppl. 1: M3), pp. 215–221, 2011. http://Benthamopen.com/tomsj/articles/V005/SI0203TOMSJ/215TOMSJ.pdf
89. Albertus, Paul, et al.: Identifying Capacity Limitations in the Li/Oxygen Battery Using Experiments and Modeling. J. Electrochem. Soc., vol. 158, no. 3, 2011, pp. A343–A351.
90. Wang, Deyu, et al.: High Capacity Pouch-Type Li-Air Batteries. J. Electrochem. Soc., vol. 157, no. 7, pp. A760–A764, 2010.
91. Padbury, Richard; and Zhang, Xiangwu: Lithium—Oxygen Batteries—Limiting Factors That Affect Performance. J. Power Sources, vol. 196, 2011, pp. 4436–4444.
92. Kraytsberg, Alexander; and Ein-Eli, Yair: Review on Li-Air Batteries—Opportunities, Limitations and Perspective. J. Power Sources, vol. 196, 2011, pp. 886–893.
93. Christensen, Jake, et al.: A Critical Review of Li/Air Batteries. J. Electrochem. Soc., vol. 159, no. 2, 2012, pp. R1–R30.

94. Williams, Mike: Rice Researchers Develop Paintable Battery: Technique Could Turn Any Surface Into a Lithium-Ion Battery; May Be Combined With Solar Cells. http://news.rice.edu/2012/06/28/rice-researchers-develop-paintable-battery-2/ Accessed Aug. 5, 2014.
95. Strasik, M., et al.: Design, Fabrication, and Test of a 5-kWh/100-kW Flywheel Energy Storage Utilizing a High-Temperature Superconducting Bearing. IEEE Trans. Appl. Superconductivity, vol. 17, no. 2, 2007, p. 2133.
96. Koh, Heebyung; and Magee, Christopher L.: A Functional Approach for Studying Technological Progress: Extension to Energy Technology. Technol. Forecast. Soc. Change, vol. 75, 2008, pp. 735–758.
97. Kascak, P., et al.: Modeling and Optimization of a MXER Tether Power System. Proceedings of the 2005 JANNAF Conference, Monterey, CA, 2005.
98. Burke, A.: Ultracapacitor Technologies and Application in Hybrid and Electric Vehicles. Int. J. Energy Res., vol. 34, 2010, pp. 133–151.
99. Halper, Marin S.; and Ellenbogen, J.C.: Supercapacitors: A Brief Overview. MITRE Nanosystems Group No. MPe05W0000272, 2006.
100. Chen, Wei, et al.: High-Performance Nanostructured Supercapacitors on a Sponge. Nano Lett., vol. 11, 2011, pp. 5165–5172.
101. Liu, C, et al.: Graphene-Based Supercapacitor With an Ultrahigh Energy Density. Nano Lett., vol. 10, 2010, pp. 4863–4868.
102. Lin, Y., et al.: Bulk Preparation of Holey Graphene Via Controlled Catalytic Oxidation. Nanoscale, vol. 5, no. 17, 2013, pp. 7814–7824.
103. Wang, Huanlei, et al.: Supercapacitors Based on Carbons With Tuned Porosity Derived From Paper Pulp Mill Sludge Biowaste. Carbon, vol. 57, 2013, pp. 317–328.
104. Chandrasekaran, S., et al.: Optimization of an Aircraft Power Distribution Subsystem. Virginia Polytechnic Institute and State University, Blacksburg, VA, 2002.
105. de Tenorio, Cyril: Methods for Collaborative Conceptual Design of Aircraft Power Architectures. Ph.D. Dissertation, Georgia Institute of Technology, 2010.
106. Armstrong, Michael, et al.: Stability, Transient Response, Control, and Safety of a High-Power Electric Grid for Turboelectric Propulsion of Aircraft. NASA/CR—2013-217865, 2013.